Aalborg Universitet

MULTIFUNCTIONAL TITANIUM DIOXIDE-GRAPHENE OXIDE MATERIALS FOR WATER PURIFICATION

Naknikham, Usuma

Publication date:
2019

Document Version
Publisher's PDF, also known as Version of record

Link to publication from Aalborg University

MULTIFUNCTIONAL TITANIUM DIOXIDE-GRAPHENE OXIDE MATERIALS FOR WATER PURIFICATION

BY
USUMA NAKNIKHAM

DISSERTATION SUBMITTED 2019

AALBORG UNIVERSITY
DENMARK

MULTIFUNCTIONAL TITANIUM DIOXIDE-GRAPHENE OXIDE MATERIALS FOR WATER PURIFICATION

By

Usuma Naknikham

AALBORG UNIVERSITY
DENMARK

Dissertation submitted 2019

.

CV

Usuma Naknikham was born in January, 1981, in Nakhon Si Thammarat, Thailand. She got the Bachelor' degree in Material Science: Ceramic and Materials Science from Chulalongkorn University, Bangkok in 2006. She continued her study there and got her Master's degree in Ceramic Technology, 2009. She worked as the scientist at Department of Science Service form 2009-2015 and got the scholarship to study abroad from The Royal Thai Government. She started her Ph.D. at Department of Chemistry and Bioscience in Aalborg University on January 15, 2016.

ENGLISH SUMMARY

Nanocomposites of titanium dioxide (TiO_2) and graphene oxide (GO) are interesting materials for applications in water purification, since they have excellent photocatalytic activity, chemical stability, and high surface area for the adsorption of water pollutants. Many of the previous studies have focused on the optimization of TiO_2-GO nanocomposites to improve their photocatalytic activity under UV light for the degradation of organic dyes as model pollutants. However, the proposed synthesis procedures are often complicated and costly. Moreover, common water pollutants have electronic structure and adsorption properties much different than those of organic dyes. Therefore, this study addressed the development of environment friendly preparation procedures for TiO_2-GO materials. The new materials were tested for their ability to eliminate phenol from water under simulated solar light. This study aims to give a deeper understanding of the chemical nature of TiO_2-GO nanocomposites, since the rational designing of TiO_2-GO relies on our ability to tailor the final chemical properties of these materials.

Enhanced TiO_2-GO composites were synthesized via the sol-gel method at pH 6 in a stirred mixture solution in a glass beaker at 60-100°C or in a static vessel at 100-200°C, where TiO_2 nanocrystals formed and anchored over GO sheets, due to the in-situ nucleation and growth of TiO_2 on GO plans. In addition, TiO_2 nanoparticles agglomeration and crystal size distribution were controlled by the GO loading. X-ray photoelectron spectroscopy (XPS) of our nanocomposites showed the presence of Ti-O-C bonding at the interface. Such type of interaction induces the stabilization of TiO_2 and GO during thermal treatment, i.e., it retards both TiO_2 phase transitions and GO reduction. Moreover, Ti-C bonding was observed for samples synthetized at $\geq$ 175°C. Both types of interface bonding are believed to influence the physical and chemical properties of TiO_2-GO composite materials and hence their photocatalytic performances.

The photocatalytic activity of the new materials was tested for the degradation of 10 ppm phenol under simulated solar light for 3 hours. The TiO_2-GO composite synthetized at 200°C with a GO loading of 0.05 wt% (0.05GTS-200) showed the highest photocatalytic activity: 4.6 ± 0.1 10^{-3} min^{-1}. The enhanced activity of this sample can be explained by considering its structural features. This nanocomposite combines Ti-O-C and Ti-C interface bonding, TiO_2 particles are enclosed by GO single layers or thin ribbons, and the particles contain high anatase fraction (92%) and less residual oxygen functional groups on GO (A_{C-O}/A_{C-C} and $A_{O-C=O}/A_{C-C}$ are 0.24 and 0.13, respectively). The structure of TiO_2-GO composites is also strongly influenced by the synthesis temperature and it was possible to obtain GO atomic monolayers decorated with TiO_2 nanoparticles or TiO_2–GO core-shell structures. But the latter ones are not desirable for photocatalytic applications, because they hinder the excitation of TiO_2 photocatalytic centers via visible light.

GO membranes were prepared with various thicknesses from 0.2 to 1.4 μm simply by vacuum filtering GO dispersions with defined concentration. Continuous films were obtained for nanocomposites with TiO_2 (P25) loading up to 80%. Intercalation of TiO_2 nanoparticles within GO reduces the thickness of GO nanoribbons in the membranes, but does not change the distance between GO monolayers. Therefore we expect that the membrane selectivity is preserved. These findings could stimulate further development of TiO_2-GO photocatalytic membranes.

DANSK RESUME

Nanokompositter bestående af titaniumdioxid (TiO_2) og grafenoxid (GO) er interessante materialer at anvende til oprensning af vand, pga. af deres høje katalytiske aktivitet, kemiske stabilitet, og en stor overflade hvorpå forurenede partikler kan adsorbere. Mange af de tidligere studier har fokuseret på optimering af TiO_2-GO nanokompositter for at forbedre deres UV fotokatalytiske aktivitet for at nedbryde organiske farvestoffer som model for forureningskomponenter. Synteserne til TiO_2-GO materialer er dog ofte komplicerede og omkostningstunge. Desuden har almindelige vandlige forureningsstoffer en meget anderledes elektronisk struktur og adsorption egenskaber end organiske farvestoffer. Fokus for dette studie er at udvikle miljøvenlige syntesemetoder af TiO_2-GO. De nye materialers evne til at nedbryde phenol i vand er testet med simuleret sollys. Dette studie giver desuden en dybere forståelse for TiO_2-GO nanokompositters kemiske natur, da en videreudvikling af TiO_2-GO beror på vores evne til at designe deres kemiske egenskaber.

Forbedret TiO_2-GO kompositter var fremstillet via sol-gel metoden ved pH 6 under omrøring (60-100°C) eller en i beholder uden omrøring (100-200°C) for at opnå TiO_2 nanokrystaller, som var bunder til GO lag, pga. in-situ nukleation og vækst af TiO_2 på GO lagene. Desuden kunne agglomerering og krystalstørrelsesfordeling af TiO_2 nanopartikler styres ved hjælp af GO mængden. Røntgen fotoelektronspektroskopi (XPS) af nanokompositterne viste tilstedeværelsen af Ti-O-C bindinger i overgangene mellem lagene. Disse typer af interaktioner er med til at stabilisere TiO_2 og GO når de opvarmes, idet det forhindrer TiO_2 faseovergange og en reduktion af GO. Ti-C bindinger var observeret for prøver som blev fremstillet ved temperature over 175°C. Begge typer af bindinger har stor indflydelse på TiO_2-GO fysiske-kemiske egenskaber og dermed også deres fotokatalytiske ydeevne.

Den fotokatalytiske aktivitet på de nye TiO_2-GO materialer var brugt til at nedbryde 10 ppm phenol i simuleret sollys i 3 timer. Den TiO_2-GO komposit (0.05GTS-200) med den højeste fotokatalytiske aktivitet (4.6 ± 0.1 10^{-3} min^{-1}) var fremstillet ved 200°C med GO mængde på 0.05 vægt%. De gode egenskaber ved denne prøve kan forklares med at betragte dens struktur. Denne nanokomposit består både af Ti-O-C og Ti-C bindinger i overgangen, TiO_2 partiklerne er lukket inde af et enkelt lag eller bånd af GO, den har en høj anatase fraktion (92%) og der er færre funktionelle oxygen grupper på GO (A_{C-O}/A_{C-C} og $A_{O-C=O}/A_{C-C}$ er hhv. 0.24 og 0.13). Strukturen af TiO_2-GO kompositter er også stærkt afhængig af syntesetemperatur og det var muligt at fremstille GO monolag dekoreret med TiO_2 nanopartikler og TiO_2-GO kerne-skal struktur. For fotokatalytiske anvendelse er den sidst nævnte struktur mindre attraktiv, da strukturen forhindrer synligt lys i at eksitere TiO_2's fotokatalytiske center.

GO membraner var fremstillet med tykkelser fra 0.2 til 1.4 μm ved at vakuumfiltrere bestemte koncentrationer af GO opslæmninger. Kontinuerte film var fremstillet ud af nanokompositterne med op til 80% TiO_2. Interkalering af TiO_2 nanopartikler indeni GO falder med tykkelsen af GO nanobånd i membranerne, men ændrer ikke afstanden mellem GO monolag. Membranens selektivitet antages derfor at være bevaret. Disse opdagelser vil stimulere til videreudvikling af TiO_2-GO fotokatalytiske membraner.

ACKNOWLEDGEMENTS

This thesis is submitted to the Faculty of Engineering and Science, Aalborg University in partial fulfilment of the requirement for obtaining the Ph.D. degree. The Ph.D. study was carried out from January 2016 to April 2019 in the Section of Chemistry.

I am highly grateful to my supervisor Yuanzheng Yue for his dedication and great help throughout the whole project. Over his supervision, his kindly and warm welcome eases my stay and homesickness for the entire study. I was impressed since the first day when I arrived with his care of me. I would also take this chance to greatly acknowledge my second supervisor Vittorio Boffa who has had great impact on the scientific works for his dedicated supervision. His guidance helps me to successfully fulfill my Ph.D. study. Through the frequent free discussions, I earned a lot of valuable inspirations for conducting my work.

My gratitude also goes to Giuliana Magnacca, Paola Calza and Marco Sarro for their assistance during the experiments and discussions, and also for taking care of me during my stay at di Chimica, Universitá di Torino, Torino, Italy. In addition, Lars Rosgaard Jensen for conducting RAMAN analysis and Dr. Ang Qiao from State Key Laboratory of Silicate Materials for Architectures, Wuhan University of Technology, China for XPS analysis. I also wish to thanks the technical support from Peter Kjær Kristensen for UV-Vis spectroscopy analysis and Lars Wagner Städe for HPLC analysis.

Thanks go to all the present and former colleges of the section of Chemistry, AAU for providing a functioning social and scientific working environment. I am appreciated from your assistances and had enjoyed every moment during our coffee break. I also, my appreciation goes to our secretaries and the lab technicians for the hospitality and help. Special thanks go to Dr. Maria Laura Tummino and Dr. Nerea Mascaraque Alvarez for both academic discussions and close friendship.

TABLE OF CONTENTS

CHAPTER 1. INTRODUCTION

1.1. BACKGROUND AND CHALLENGES

Over the recent years, the scarcity of drinking water has been arising as a pressing issue for the humanity. Moreover, researchers have been reporting an increasing number of water systems to be contaminated by chemical compounds arising from human activities [1–4]. These contaminants are often present at low concentrations (μg/L or ng/L) and therefore are named micropollutants. Despite their low concentrations, micropollutants cause concern for their impact on the environment and on human health, thus making water inappropriate for human consumption [5]. Most of these chemicals reach the environment through wastewater streams. In fact, over 80% of wastewater around the world is discharged without suitable treatments, as reported by UN World Water Development Report, 2017 [6]. Furthermore, traditional wastewater treatment plants are not designed for the abatement of micropollutants and their low concentration makes their abatement even more challenging [2,3]. In addition, the advanced technique in the tertiary process is still costly, chemicals adding requirement and energy consuming [3,7].

In this context, photocatalysis can provide an economic method for the abatement of micropollutants [8]. Titanium dioxide (TiO_2) is the benchmark photocatalytic material for environment applications, since it is nontoxic, chemically stable, inexpensive and presents high photocatalytic degradation rates [8–10]. However, the limitations of TiO_2 are that: (i) it is active only under the UV light (therefore it contains only 5% of the sunlight) and (ii) its efficiency in the degradation of organics is limited by the high rate of electron-hole pair recombination [9]. The combination of TiO_2 nanoparticles with other materials has been extensively investigated to come across these limitations [10,11]. Recently, the emerging of graphene oxide has allowed to design and fabricate novel hybrid TiO_2-graphene oxide photocatalysts with enhanced performances in water depollution. This new generation of photocatalysts has been proven to be effective in the abatement of micropollutants, such as dyes, pharmaceuticals and pesticides under both UV and visible light. [8,12–14] Indeed, combining TiO_2 with graphene oxide or reduced graphene oxide presents several advantages. It can lower the band gap energy of TiO_2 from 3.2eV (UV light) to the visible range [8,15]. In addition, reduced graphene oxide sheets can act as an electron acceptor, thus retarding the recombination of electron-hole pair via interfacial bonding [16]. Furthermore, graphene oxide has the ability to adsorb pollutants, and hold them close to the TiO_2 photocatalytic centers [17]. Last but not least, graphene oxide can be synthetized using natural graphite by easy and cheap methods [8].

Once proven, the high photocatalytic activity of novel TiO_2-graphene oxide nanocomposite materials has had many studies dedicated to their optimization.

Generally, in-situ sol-gel synthesis of TiO_2 is emphasized to obtain good chemical bonding between the oxide nanoparticles and graphene oxide planes. In addition, hydrothermal curing and annealing processes, can result in the partial reduction of the graphene oxide, in increasing the TiO_2 crystallinity, and in strengthening the interface bonding between the two materials [18,19]. On the other hand, solvothermal and chemical reduction of graphene oxide was reported to induce the reduction of the graphene oxide sheets, which can anchor to the TiO_2 nanoparticles with no adhesion. by using the specific chemical such as hydrazine and hydroquinone [12]. All of these methods consume more energy and are chemically hazardous, thus being of concern to the environmental effects. However, the most important route is the sol-gel nucleation and growth, since it needs mild conditions and simple set-up [20]. This method enables flexible functionalization with other metal ions and molecules and the homogeny of dispersion, and also particle size distribution of TiO_2 via controlling the rate of reaction [20]. In addition, the method ensures the interface bonding by growing TiO_2 nanoparticles on graphene oxide planes via the oxygen functional nucleation sites [21–23]. Moreover, controlling pH brings about the the strong electrostatic interaction between the positive and negative charges on the surface of graphene oxide and TiO_2 [20,24]. In addition, the hydrolysis and hydrothermal methods are suitable for realizing TiO_2-graphene oxide synthesis, since they enable the interface bonding between graphene oxide and TiO_2 and easy to control the reduction degree of the graphene oxide. Moreover, both methods cause less contamination since the reaction occurs in water [19,25]. In addition, the excessive loading of graphene oxide to TiO_2 could hinder the photocatalytic reaction because graphene oxide absorbs more light and shields TiO_2 nanoparticles from light excitation [16,26,27]. Furthermore, the photocatalytic activity of TiO_2-graphene oxide nanocomposites is a complicated phenomenon, as it is influenced by many factors such as the morphology of both materials, the interface bonding, the reduction of graphene oxide, the preparation method and the conditions of the photocatalytic testing.

Hence, this thesis focuses on the impact of the incorporation of graphene oxide into TiO_2 on chemical and physical behaviors of novel TiO_2-graphene oxide based photocatalytic materials in term of organic pollutant elimination from wastewater treatment. TiO_2-graphene oxide was synthesised via the simple sol-gel synthesis with the environmental friendly chemicals and conditions. The hydrolysis and hydrothermal reactions were conducted to produce the TiO_2-graphene oxide nano-composites. Stronger interaction can be created between the two materials by performing the thermal treatments and the progressive reduction on graphene oxides. The amount of graphene oxide loading (50 wt%) was used to study the mutual effect of interface bonding on the morphology and the thermal behaviour of the composites. In addition, the influence of graphene oxide loading and high temperature treatment on the photocatalytic activity was studied by varying the amount of graphene oxide loading from 0-1 wt%. Phenol was used as a pollutant molecule to study removal of the pollutants under sun simulator. Most of the

photocatalytic characterizations were conducted with several dye solutions under UV or UV-VIS light [28–30]. However, precaution has to be taken regarding phenol, since it is a source of contamination in water, and it is harmful for human and other organisms as mentioned before. The TiO_2 photocatalysts are effective for reducing the fouling problem on graphene oxide membrane, and make the organic substances degraded [31]. Therefore, the graphene oxide membrane bearing the TiO_2 powder was systematically tested in this project. In addition, the separation of the photocatalytic nanopowder from the wastewater treatment plant for recovery is not easy [32], however, the TiO_2-GO membranes could be potentially used to realize such separation.

1.2. OBJECTIVES

This Ph.D. project aims to develop novel TiO_2-graphene oxide nanocomposite materials with outstanding photocatalytic activity for abatement of organic compounds under solar light.

The specific objectives of this project are summarized as follows.

(1)   To study the effect of chemical bonding in TiO_2-graphene oxide materials on morphology and thermal behavior.

(2)   To study how synthesis parameters can affect the morphology and photocatalytic activity of the final TiO_2-graphene oxide nanocomposites. High emphasis will be given to the study of TiO_2-graphene oxide interphase, since this interphase can highly affect the photocatalytic activities of the nanocomposites

(3)   To investigate the possibility to apply the new materials in the fabrication of photocatalytic membranes with self-cleaning ability.

1.3. THESIS CONTENT

Part of this research work is compiled into three papers. The thesis is thus a combination of these manuscripts, and six chapters that describe additional findings and give a more detailed picture of this PhD project.

The articles, which are listed here, can be found at the end of the thesis as Paper I, II and III:

I.   **U. Naknikham**, V. Boffa, G. Magnacca, A. Qiao, L. R. Jensen, Y. Yue, 2017, "Mutual-stabilization in chemically bonded graphene oxide–TiO_2 heterostructures synthesized by a sol–gel approach", *RSC Advances*, 7, 41217-41227 (2016).

II. **U. Naknikham**, G. Magnacca, A. Qiao, P.K. Kristensen, V. Boffa, Y. Yue, "Phenol abatement by titanium dioxide photocatalysts: effect of the graphene oxide loading" (under review).

III. **U. Naknikham**, G. Magnacca, A. Qiao, P.K. Kristensen, V. Boffa, Y. Yue, "Phenol Abatement by GO-TiO$_2$ and rGO-TiO$_2$ Photocatalsts (to be submitted).

CHAPTER 2.
THEORETICAL BACKGROUND

In the following chapter, graphene oxide structure, transport in graphene oxide membranes, sol-gel synthesis of TiO_2 nanoparticles, functioning of TiO_2-based and TiO_2-graphene oxide photocatalysts, and synergistic effects in TiO_2-graphene oxide photocatalytic membranes are basically explained including the preparation methods and the characterizations.

2.1. GRAPHENE OXIDE STRUCTURE AND PROPERTIES

Graphene is the youngest carbon material, since it was discovered in 2004. Graphene is a two dimension (2D) single-layer of hexagonal carbon framework with one atomic thickness [33–36]. A single layer graphene can be shaped into various forms: e.g. by wrapping into 0D buckyball (fullerenes), rolling into 1D nanotubes, and stacked into 3D graphite as shown in Figure 2-1 [35]. Although, these materials originate from carbon atoms arranged into a honeycomb network, their properties are different.
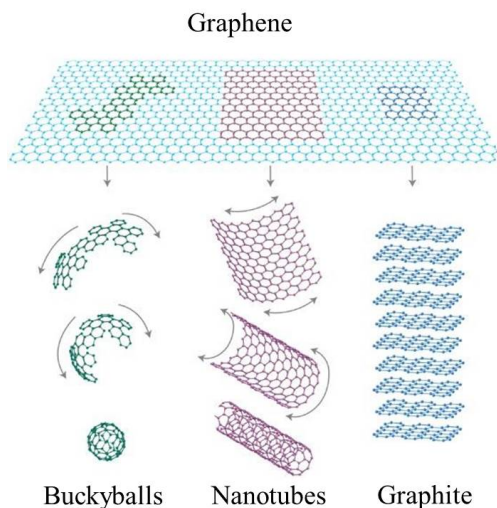
Figure 2-1 Carbon family materials; graphene oxide, fullerenes, nanotubes and graphite. The figure is reproduced with permission from Springer Nature [35].

The rise of graphene has unlocked new exciting directions in a broad area of research, because when compared with traditional materials, it exhibits superior

physical and chemical properties. For example, graphene has a high specific surface area (theoretically 2,630 m^2/g for single-layer graphene), zero band gap energy, high electron mobility, high electrical and thermal conductivity, and chemical stability [34,36,37]. However, large-scale production and processing remain a challenge for graphene. On the contrary, graphene oxide can be easily derived from natural graphite by chemical oxidation and exfoliation in water or in organic solvents. During this process, the stacking structure of graphite turns into a dispersion of graphene oxide monolayers, as shown in Figure 2-2. Graphene oxide structure consists of a carbon sheet decorated with various types of functional groups, including phenol, hydroxyl and epoxide on the basal plane and carboxyl group at the edges. The presence of oxygen functional groups on graphene oxide sheets results in strong hydrophilic properties, which make this material easy to disperse in water and to be functionalized [34]. In addition, graphene oxide can be partially reduced to graphene-like structures (reduced graphene oxide) by thermal or chemical treatments [38–40] .
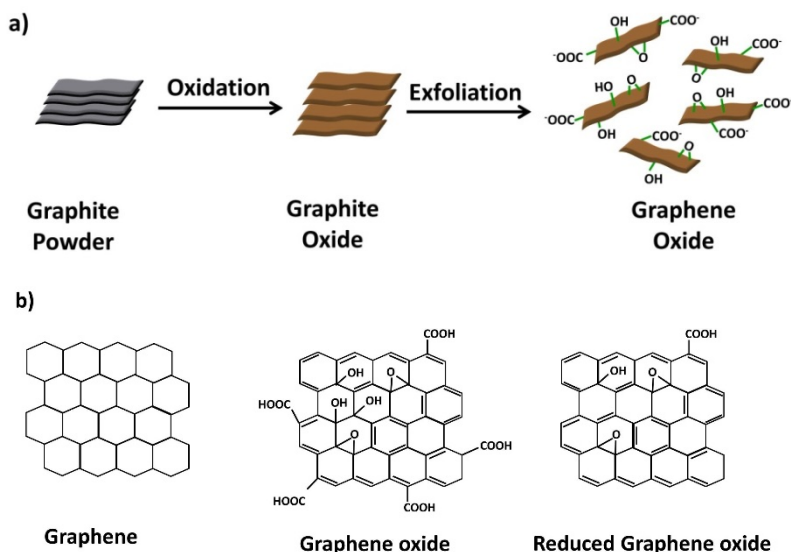
Figure 2-2 a) Schematic of graphene oxide preparation and b) lattice structure of graphene, graphene oxide and reduced graphene oxide based on reference [41] and [42], respectively.

For these reasons, graphene oxide and graphene oxide-based materials are applied in many fields [36,37];

- Environmental applications [18]: water and air filtration, membrane, desalination, adsorbent, capacitive deionization, antimicrobial, electrodes for environmental sensing.

- Energy applications: energy conversion and storage, solar cell, optoelectronic and sensing applications, fuel cells, photovoltaic devices.
- Medical applications [41,43]; injectable cellular labeling agents, drug delivery systems, and scaffold reinforcements.
- Other fields: anti-friction and lubricity, coatings and flame retarder, filler [44].

In this study, graphene oxide powder was synthesized via a modified Hummers method [45] and natural graphite powder was used as starting material. A detailed description of the synthesis procedure for the preparation of the graphene oxide dispersions used in this work is reported in Paper I. After synthesis, graphene oxide was freeze-dried, obtaining a powder that was readily dispersible in water. In this thesis, this product hereafter will be called GO.

2.1.1. MICROSTRUCTURE OF GRAPHENE OXIDE

The microstructure of GO was investigated by scanning electron microscope, SEM (Zeiss, 1540 XB). Figure 2-3 shows the typical open sponge-like structure of freeze-dried GO [37,46].
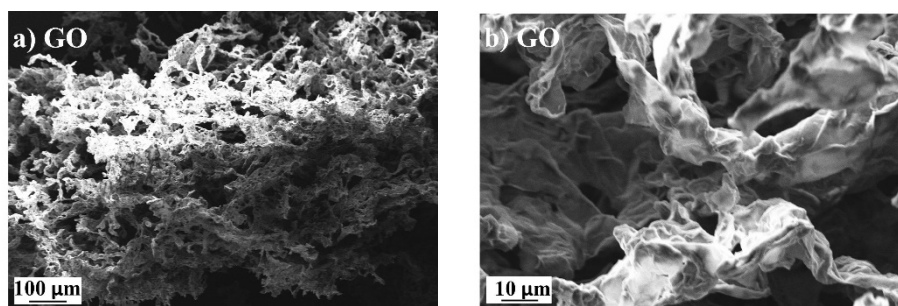
Figure 2-3 SEM images of the sponge like structure of freeze-dried GO at two different magnifications (a and b). The micrograph b) is reproduced from Paper I with permission from the Royal Society of Chemistry.

X-rays diffraction (XRD) (PANanalytical Empyrean Diffractometer) was used to confirm that all the starting graphite was converted to GO during synthesis (Figures 2-4). The position of starting GO peak is observed at $2\theta = 10.46°$ corresponding to a distance of 8.45 Å between GO monolayers, while the characteristic peak of graphite is centered at $2\theta = 26.46°$, corresponding to a d-space of 3.72 Å. GO has a wider interlayer distance, because it consists of highly oxidized carbon sheets, whose stacking is not as efficient as for the graphene sheets in graphite. In addition, the highly ordered structure of the graphite compared to GO results in a different thickness of stacked domains, which was estimated to be 45 nm and 33 nm, for

graphite and GO, respectively. This distance was calculated with the Scherrer equation [47] (equation 2-1):

$$d = \frac{\beta\lambda}{\omega cos\theta} \qquad\qquad 2-1$$

where λ is the X-ray wavelength, 1.5406 Å (CuKα), ω is the full width at half maximum intensity (FWHM) of the peak, θ is the diffraction angle, and the shape factor (β) in the case of graphite-like structure is 1.84 [48].
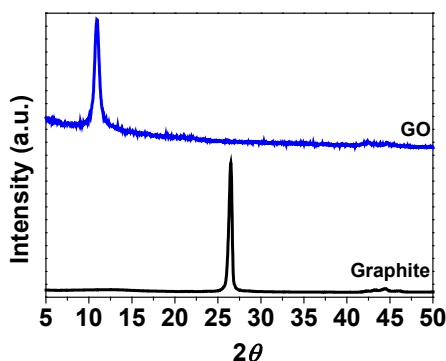
Figure 2-4 XRD patterns of GO and graphite. The Figure reproduced from Paper I with permission from the Royal Society of Chemistry.

2.1.2. CHEMICAL PROPERTIES OF GRAPHENE OXIDE

As mentioned earlier, graphene oxide is synthesized by the oxidation of natural graphite. As a results of this oxidation, the graphene oxide sheets are decorated with different types of oxygen functional groups: carboxyl (-COOH), hydroxyl (-OH), carbonyl (C=O) and epoxy (-C-O-C-) [9,18]. Therefore, spectroscopy techniques such as Flourier Transform Infrared spectroscopy (FT-IR), Raman spectroscopy and X-ray photoelectron spectroscopy (XPS) were used for studying the chemical structure of graphene oxide.

Figure 2-5a shows the FT-IR spectrum of our GO powder. The signal of the aromatic skeleton is centered at 856 cm^{-1} [49,50]. Nevertheless, in this spectrum we can see also several peaks, which are typical of the oxygen functions in GO. Those peaks include the stretching of carbonyl (C=O) at 1731 cm^{-1}, the -OH bending of GO hydroxyl and water at 1618 cm^{-1}, the carboxyl (C-O-H) at 1384 cm^{-1}, the signal of the epoxy groups at 1224 cm^{-1}, and the -OH stretching of phenol groups at 1170 cm^{-1}. Moreover, the material is highly hydrophilic and we can observe the broad peak of water –OH stretching at around 3200-3400 cm^{-1}.
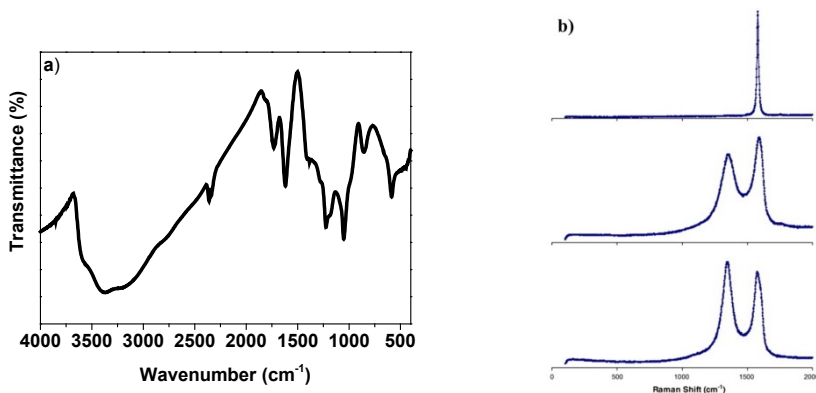
Figure 2-5 a) FT-IR spectrum of GO and b) RAMAN spectra of graphite (top), GO (middle) and reduced GO (rGO, bottom) [39].

Raman is a spectroscopic technique largely used for studying the structures of carbon materials. The typical Raman spectra of graphite, graphene oxide and reduced graphene oxide are shown in Figure 2-5b. The Raman shift of graphite shows only G peak at 1581cm^{-1} which indicated well-ordered graphite. While, graphene oxide shows 2 main peaks at 1363 and 1594 cm^{-1}, which correspond to the D and G bands, respectively. The G band relates to sp^2 carbon band [39] while D band indicates sp^3 carbon band. The G and D bands are also present in the spectrum of the reduced graphene oxide. However, the reduction of graphene oxide can be revealed by an increase of the intensity ratio between G and D band (I_D/I_G) [51].

XPS was used to study the chemical composition and chemical bonding of pure GO and of the nanocomposite materials. The C1*s* and O1*s* XPS spectra of GO are shown in Figure 2-6.
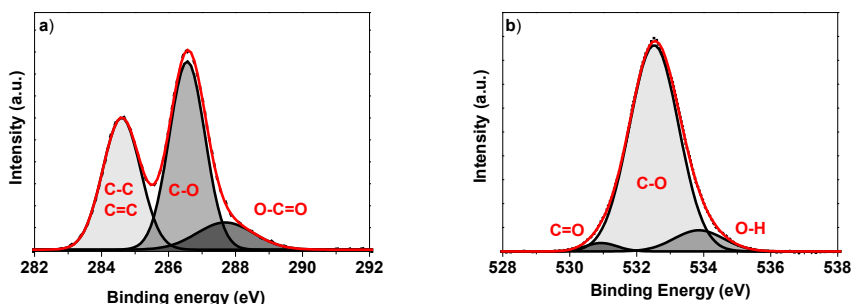
Figure 2-6 XPS spectra of GO a) C1s and b) O1s. The dotted black line presents the measured spectra and grey peaks present the component peaks of the fitted spectra (red).

In both cases, the deconvolution technique is used for analyzing the peak components. The C1*s* spectrum in Figure 2-6a is deconvoluted into 3 peaks with characteristic binding energies, which correspond to the aromatic carbon (sp^2) at

284.3 eV ,C-O at 286.5 eV and C=O (or O-C=O) at 287.7 eV [52]. The deconvolution of O1s spectrum in Figure 2-6b shows peaks at binding energy of 530.9, 532.5 and 533.9 eV that represent C=O, C-O and O-H, respectively [53].

2.1.3. THERMAL PROPERTIES OF GRAPHENE OXIDE

After synthesis, graphene oxide is a metastable material that can slowly be reduced to graphene like-structure even at room temperature [54]. Therefore, its thermal stability must be considered. The thermal stability of graphene oxide is here studied by the means of differential scanning calorimetry and thermogravimetry, in the temperature range between 50 and 800°C under argon atmosphere. The plot of the heat flow (DSC) and weight loss (TG) as a function of the temperature for GO is shown in Figure 2-7a. The mass loss curve of GO presents in 3 main steps. The first one, ranging from room temperature to 150°C, is due to the evaporation of physisorbed water. The second step is the degradation of functional groups between 150-350°C. During this step, water is released from dehydration reactions, and CO or CO_2 from decarbonation reactions [55]. The last decomposition that takes place above 350°C is due to the degradation of the carbon skeleton [55,56] and of the residual oxygen functional groups [57]. These processes are confirmed by the DSC curve, where we can observe the endothermic evaporation of water below 150°C and an exothermic peak with maximum at 187°C, which corresponds to the GO thermal reduction [58].
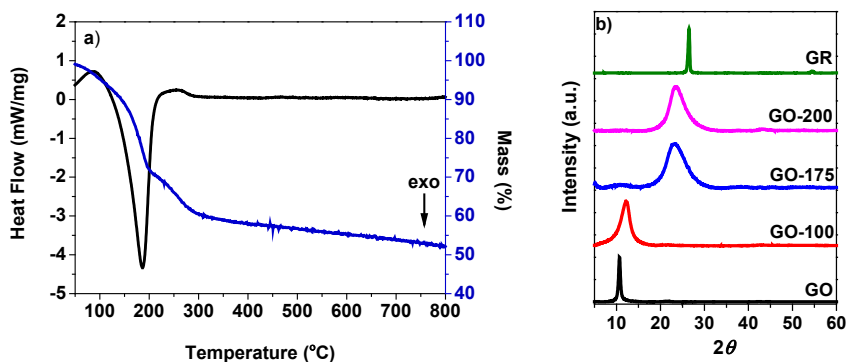
Figure 2-7 a) Thermal analysis of pure GO and b) XRD patterns of graphite (GR), GO and GO treated from 100-200°C for 4 hours (the sample names are GO followed by the treatment temperature e.g.GO-100 is GO is treated at 100°C). Figure b) is taken from Paper III.

According to the results from thermal analysis, GO was treated at different temperatures from 100-200°C for studying the reduction stages by XRD analysis. The patterns of graphite, graphene oxide and thermal treated GO are shown in Figure 2-7b. The graphite peak is at 2θ = 26.44 corresponding to d-spacing at 3.72

Å. Meanwhile, the main peak of GO appears at 2θ = 10.46 referring to *d*-spacing = 8.27Å, as discussed above [59]. After hydrothermal treatment, the peak of GO moves towards higher angles: from 2θ = 10.7° to 2θ = 23.9° (for materials treated at 100 and 200°C, respectively). In addition, this peak becomes broaden after increasing the treatment temperature up to 175°C. This is a consequence of the fact that the partial chemical reduction of GO causes a re-stacking of the carbon sheets in thin ribbons, which can form irregular or cyclic structures, as discussed in paper III. Above 175°C, the XRD peak becomes narrow again, meaning that the reduced GO is converted to a more ordered (graphite-like) state.

2.2. TRANSPORT IN GRAPHENE OXIDE MEMBRANES

Recently, a large number of nanomaterials such as titanium dioxide, surfactant-templated silica, zeolite, graphene, MOFs (metal organic framework), LDHs (layered double hydroxide), layered silicates, etc. have been applied for the fabrication of artificial membranes for water purification [60]. Among these materials, graphene and its derivatives have very distinct properties, such as flexibility, mechanical strength [61], low cost, and they are amenable to scale up [60,62].

There are two kinds of graphene-based membrane; I) nanoporous graphene membranes and II) stacked graphene oxide membranes. Although, nanoporous graphene membranes show outstanding water permeability and high rejection towards a large variety of organic molecules and metallic ions, their fabrication on a large scale remains a problem. On the other hand, the permeability of stacked graphene oxide membrane is similar to that of the porous graphene membranes but their fabrication is much easier, and can be attained with simple processes, such as vacuum filtration or blade coating [18]. Indeed, graphene oxide can form highly stable dispersions in water without agglomeration due to the mutual repulsion of the negative charge functional groups [60]. For instance, controlling the volume or the concentration of graphene oxide suspensions; Lui, H. *et al.* [63] were able to fabricate free standing graphene oxide membranes with controlled thickness between 20 and 200 nm by the filtration method. Nair, R. R. *et al*. [64] fabricated free standing graphene oxide films with thickness of 1 μm (Figure 2-8a and 2-8b), and demonstrated that only water vapor passes through these films, while hexane, ethanol and even helium are blocked (Figure 2-8c and 2-8d). On the other hand, water vapor cannot permeate through reduced graphene oxide.

Transport thought graphene oxide membranes is rather complex (Figure 2-8e). It includes the contribution of wrinkles and nanopores, but it is mainly due to the interspacing between graphene oxide sheets. In a consolidate membranes, graphene oxide sheets piles in a parallel manner, forming 3-5 Å empty interspacing (nanocapillaries) between non-oxidized regions (graphene domains). It has been proposed that these nanocapollaries can host a monolayer of water molecules, which

can permeate through the membranes at an exceptional rate [64]. However, Wei, N. *et al* [65] argue that this fast water transport through pristine graphene channels is in fact prohibited by interaction of water molecules with the lateral oxide regions. Moreover, water molecules can form H-bond with the oxide functions. As a consequence, the interlayer space (d) can increase from 7 to above 10 Å [18], thus changing both the permeability and the selectivity of the graphene oxide membrane [60,66–69].
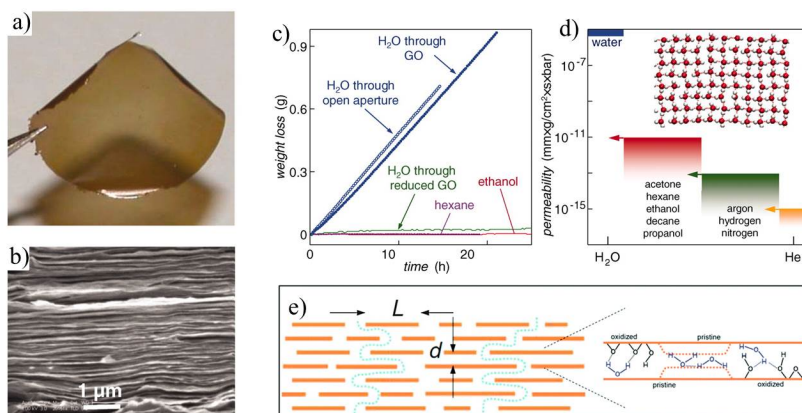
Figure 2-8 a) The photo of free standing graphene oxide with 1µm thickness, b) the SEM photo of thin film cross section, c) the weight loss from the container covered with/without graphene oxide film and reduced graphene oxide of the target molecule in the period of time, d) the permeably of various gases, water and alcohols vapors, and e) the schematic of water transportation pass the inter layer of graphene oxide. The figures are reproduced with the permission from the Advancement of Science [64].

2.3. SOL-GEL SYNTHESIS OF TITANIUM DIOXIDE NANOPARTICLES

Since TiO_2 was discovered in 1795 and brought to commercial production in the 1920s, it has been used for broad range of applications, such as a pigment and opaque agent in paints, as additive for plastics, paper, textiles, inks, cosmetic, and in corrosion-resistant coatings [70], due to its low cost, non-toxicity and high chemical stability [71] .

TiO_2 is a polymorphic material, having three main crystal structures (Figure 2-9a) that are tetragonal for anatase and rutile, and orthorhombic for brookite. In general, anatase and rutile are found in nature. On the contrary, brookite is obtained by chemical synthesis. The XRD diffractograms in Figure 2-9b show the fingerprints of tree crystal structures of TiO_2.
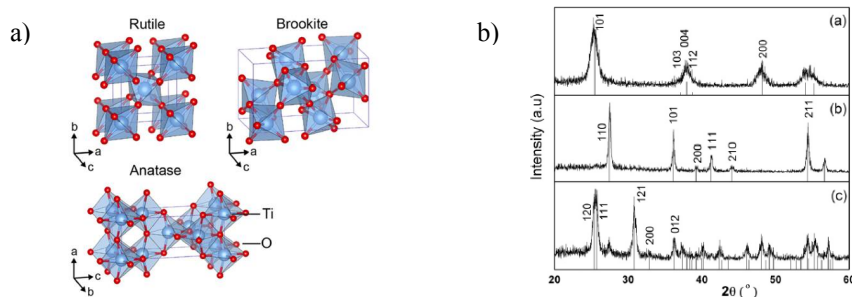
Figure 2-9 a) crystal structures of TiO₂ polymorphs [72] and b) XRD patterns of (a) anatase, (b) rutile and (c) brookite [70,73].

The synthesis of TiO_2, especially in the form of micro- and nano-particles, can be performed via various chemical routes such as hydrolysis, sol-gel, micro-emulsion, solvo/hydrothermal, chemical vapor deposition, electrodeposition techniques [74,75]. Among those methods, sol-gel synthesis is the most worth and widely used technique for the synthesis of TiO_2 nanoparticles, because it is simple and can be done at ambient temperature and pressure, and does not require a complex set-up. In addition, the synthesis reaction can be controlled easily by limiting the water in the reaction mixture (i.e. by controlling the hydrolysis reaction rate), and by controlling the TiO_2 precursor concentration, pH and temperature. Therefore, this method provides high reproducibility, and makes possible to obtain narrow particle size distribution, and to control the crystal phase, allowing the synthesis of both single and mixed phases. Moreover the sol-gel method permits to obtain highly pure materials, to avoid contamination, and is flexible for doping with other ions [76].

In general, sol-gel synthesis of TiO_2 can be performed via two routes, as the TiO_2 precursor can be an alkoxide (e.g. titanium (IV) isopropoxide) in alcohol or an inorganic compound (e.g. $TiCl_4$) added to water. After hydrolysis and condensation reactions of the titanium precursor, a colloidal suspension (sol) is formed. Then, drying and heat treatment are conducted to obtain TiO_2 materials with designed properties [77,78]. The titanium alkoxide precursors are still costly for being used in the commercial production of TiO_2 [70]. Moreover, the synthesis process needs the special set-up, due to their sensitivity to moisture and the organic solvents [79,80]. Meanwhile, the aqueous route of $TiCl_4$ is widely used for TiO_2 commercial production [70], since it is easier and less expensive than the alkoxide route [81], and allows to obtain target phases [82]. For instance, pure rutile can be synthesized by adjusting the molar ratio of $TiCl_4$, ethanol and water at 50°C [82]. Zheng, W. *et al*. [83] prepared mixed anatase-rutile nanoparticle by hydrolysis of $TiCl_4$ in hydrochloric acid in the presence of 1-ethyl-3-methyl-imidazolium bromide. When the hydrolysis of $TiCl_4$ is performed in basic environment (pH 8), the anatase phase can be obtained [79].

In this study, TiO_2 nanoparticles were obtained by the sol-gel synthesis, using $TiCl_4$ as ceramic precursor. During synthesis, the pH of suspension was maintained at 6 by adding NH_4OH to facilitate the interaction with GO sheets during the synthesis of composites. The details of the syntheses are written in Paper I and Paper III. The syntheses were conducted by stirring the suspension in a flask (TD materials) at 60°C and 100°C, or under hydrothermal conditions (TS materials) from 100°C to 200°C. The morphology of some of the TiO_2 nanoparticles synthesized in this PhD project is shown in Figure 2-10, where the samples are named according to their synthesis method and temperature.

High resolution TEM images of pure TiO_2 synthesized at 100°C in the stirred flask using the static hydrolysis method (TD-100 and TS-100, respectively) show highly agglomerated polyhedral crystals with size of 5-10 nm (Figures 2-10a and 2-10b). Moreover, the crystals in both figures present lattice spacing of 0.35 nm, which can be related to the (101) plane of the anatase phase [84]. Unfortunately, it is not possible to exclude brookite, since it has similar lattice distance (0.346 nm) for the plane (111) [41]. Therefore, the finger prints of anatase (A) and brookite (B) were checked in the XRD diffractograms of these powders, which are presented in Figure 2-10c, together with those of samples synthetized at other temperatures. When we exclude the sample prepared at 60°C, namely TD-60, which is largely amorphous, all the other samples consist mainly of anatase crystals (A), which are mixed with brookite (B). The main peak of TiO_2 ($2\theta = 25.2°$) is used to determine the size of the anatase crystallites by the Sherrer equation in equation 2-1 (the shape factor (β) is 0.84), while the weight fraction of the anatase phase is calculated as explained in Paper I. Hence, crystallite size and anatase fraction are plotted vs synthesis temperature in Figure 2-10d. TiO_2 samples prepared at 100°C have an average crystallite size of about 8 nm and anatase fraction of nearly 80%, regardless of the preparation method. In addition, anatase crystal size and weight fraction increase with temperature. Moreover, brookite is still maintained in all of temperature. The formation of mixed phase anatase – brookite has been already reported [75,85]. For instance, Mutuma, B. K. *et al*. [75] found that the anatase-brookite ratio is controlled by the pH of the synthesis mixture, and the amount of anatase and eventually rutile increase with the calcination temperature. In addition, the brookite phase is still present after the calcination temperature up to 200°C. Hu, Y *et al*. [86] reported similar results: the fraction of brookite increases when synthesis pH decreases. Moreover, urea and citric acid can be used to control the anatase weight ratio [84,85].
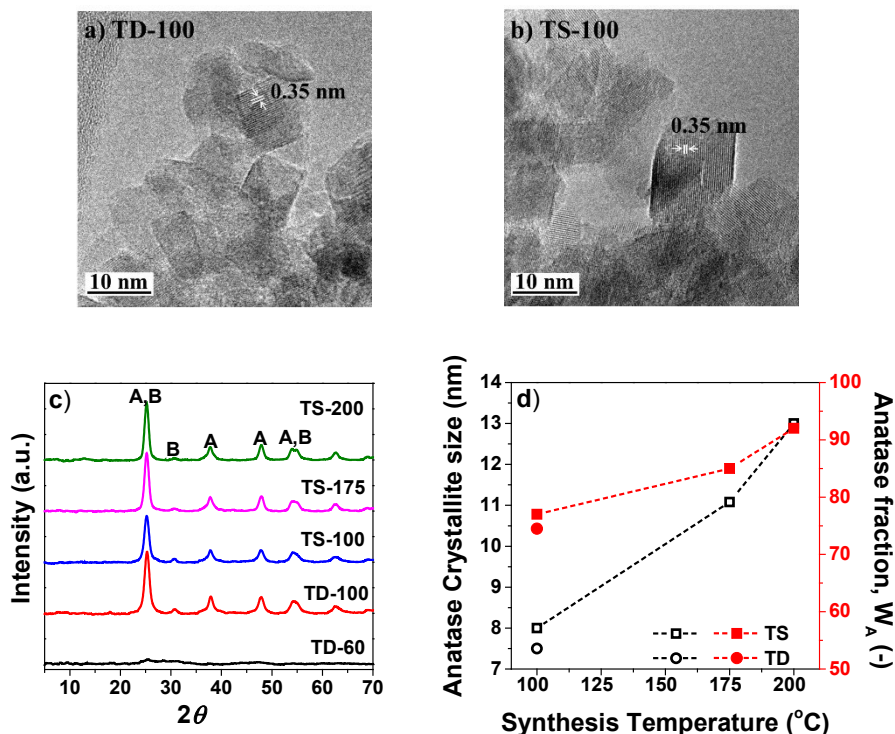
Figure 2-10 HR-TEM pictures of a) TD-100 and b) TS-100. c) The XRD patterns of pure TiO$_2$ powders prepared at different temperatures (A and B represent to anatase (PDF 01-121-1272) and brookite (01-029-1360) characteristic peaks, respectively). d) The crystal size and weight fraction of anatase were calculated by Scherrer's equation.

2.4. FUNCTIONING OF TIO$_2$-BASED AND TIO$_2$-GRAPHENE OXIDE PHOTOCATALYSTS

The widespread interest in photocatalysis started when Fujishima and Honda found that TiO$_2$ can split water under sunlight in 1972 [70]. Since then, TiO$_2$ has been the most commonly used photocatalytic materials in many applications, such as water treatment, self-cleaning material and air purification technologies. In addition, the semiconductor properties of TiO$_2$ for its application in advanced technologies, such as rechargeable batteries, super capacitors and sensor devices [70], dye-sensitized solar cells and biomedical applications [74]. However, most of the recent publications on TiO$_2$ still concern the abatement of organic pollutants like dyes [70], pesticide [11], phenols and other aromatic compounds [87].

TiO$_2$ is a semiconductor material with a band gap of around 3.0-3.2 eV, depending on the crystalline phase [11,70]. Therefore, it can be activated as photocatalyst by

UV light. For instance, anatase has band gap energy (BG) of 3.2 eV and therefore a light with wavelength smaller than 387 nm (UV light) is required for exciting an electron from conduction band (CB) to valence band (VB) [11], as shown in Figure 2-11. After the electron-hole pairs migrates to TiO_2 surface, various redox reactions can occur, for instance i) the oxidation of H_2O by an hole (h^+) to form hydroxyl radicals ($OH^{\bullet}$) and ii) the reduction of O_2 to obtain superoxide radical anions ($O_2^{\bullet-}$). Both $OH^{\bullet}$ and $O_2^{\bullet-}$ are powerful radical species, which can oxidize organic compounds, eventually yielding CO_2 and H_2O [11,71].
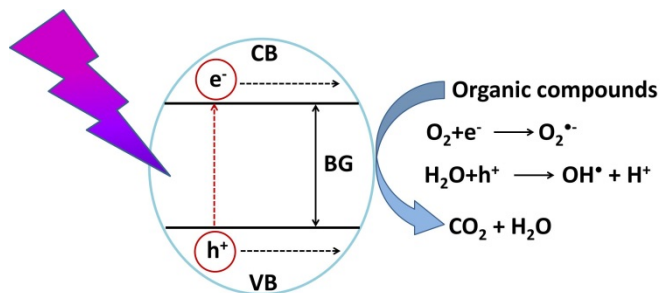
Figure 2-11 Schematic of TiO₂ photocatalytic reaction under UV light based on reference [11,71].

Compared to rutile phase, anatase suits for photocatalytic applications because it has higher surface area and photodegradation activity and stability [10]. It was explained that rutile exhibits higher rate of electron-hole pairs recombination. In addition, rutile is the thermally stable phase, thus it pronounces to bigger size and lower surface area that is the important role in photocatalytic reaction [84,88,89]. Moreover, anatase also has advantages over brookite, e.g., it is easy to be synthesized [10]. However, anatase has excellent photoreaction ability only under UV range due to the wide energy band gap and shows fast recombination rate of electron-hole pairs. Both factors limit its spectrum of applications. Above all, anatase TiO_2 has a scarce activity under sunlight, which consists of about 45% of visible radiation, and only 2-5% of UV light [10]. Therefore, various modifications have been proposed for TiO_2 materials to enhance their photocatalytic activity under the visible light and for retarding the recombination rate of electron-hole pairs [8].

TiO_2 materials have been modified for narrowing the band gap by doping with others metals (Cu, Ag, Fe, V), non-metal atoms (N, C, O), by combining with others semiconductors (ZnO, CdS, Bi_2O_3) [10,11] and by developing TiO_2 mixed phases (anatase-rutile, anatase-brookite system) [75,84]. Such modification includes the use of carbon materials: fullerenes, carbon nanotube and graphene [8]. However, graphene-TiO_2 semiconductors have high potential to be the photocatalytic materials for the future, since graphene possesses high electron mobility, large surface area and flexibility for functionalization [8,12]. Hence, graphene derivatives can enhance

the photodegradation performances of TiO_2 photocatalyst systems in several ways: (i) by adsorbing the pollutants and holding them close to the TiO_2 photocatalyst surface [17]; (ii) by retarding the electron-hole recombination as the separated charge is transferred from the TiO_2 surface to the graphene plane via interface bonding; (iii) by extending the absorption range to visible light, due to narrowing of band gap energy, as a result of the formation of Ti-O-C or Ti-C at the interface [8,12,90,91]. Figure 2-12 shows the photocatalytic reaction of TiO_2-graphene composite materials under visible light.
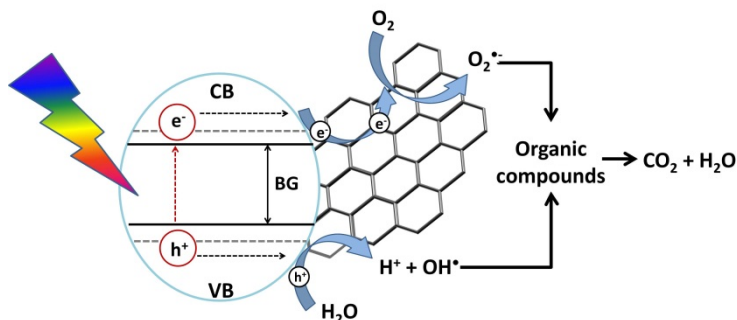
Figure 2-12 Schematic of TiO$_2$-graphene photocatalytic reaction based on reference [8,12,92].

2.5. SYNERGISTIC EFFECTS IN TIO$_2$-GRAPHENE OXIDE PHOTOCATALYTIC MEMBRANES

As mention in paragraph 2.2, graphene oxide multilayer membranes are attracting attention to fabricate devices for water filtration and purification. However, fouling (i.e. the membrane get dirty during filtration) is still a problem for graphene oxide-based membranes and for membrane technology in general, because it limits the efficiency of the filtration process and it makes necessary frequent cleaning cycles [93,94]. Moreover, organic pollutants can accumulate on the membrane surface (concentration polarization) at the detriment of both membrane selectivity and permeability [95]. Hence, functionalization of graphene oxide membranes with photocatalytic materials could solve those problems [93]. We can imagine that integration of TiO_2 nanoparticles in graphene oxide membrane can produce the same synergistic effects that are described above for the photocatalytic particles. As the photocatalytic material, TiO_2 gives the self-cleaning effect avoiding the fouling problem, meanwhile the organic molecules are degraded on top of the membrane, when its surface is exposed to UV or visible light [32]. In addition, water permeability increases since intercalation of TiO_2 particle between graphene oxide planes can create a more open structure than in pristine graphene oxide membrane

[38,94]. The model of a TiO_2-graphene oxide photocatalytic membrane can be seen in Figure 2-13.
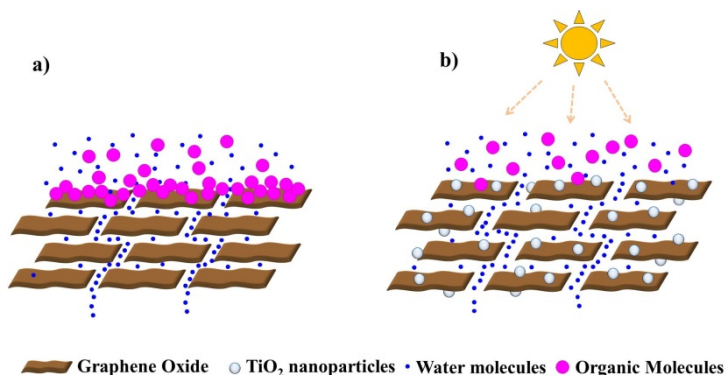
Figure 2-13 Schematic of a) graphene oxide membrane and b) TiO_2-graphene oxide membrane based on reference [16 and 71].

Zhu, C. *et al*. [93] insert 50 nm TiO_2 particles into graphene oxide membranes and found that the average space between graphene oxide plans was increased. Their experiments showed that under UV-light the graphene oxide/TiO_2 membrane can obtain 92% methylene blue degradation and after fouling the water flux recoverability was 96%. Moreover, a commercial polymeric membrane has been modified with graphene oxide-TiO_2 thin film obtaining 22.4 L $m^{-2}h^{-1}$ water flux at 0.4 MPa and 98.8% $NaSO_4$ rejection. Also, graphene oxide-TiO_2 multilayers films supported on polymer membranes improved the antifouling property of dye solutions such reactive red 48, reactive back 5 [96]. The coating of a ~ 65 μm graphene oxide-TiO_2 layer over commercial ultrafiltration membranes allowed to achieve higher water flux than traditional nanofiltration and reverse osmosis membranes, and to remove diphenhydramine (pharmaceutical compounds) and methyl orange under near-UV/Vis light [97].

CHAPTER 3.
SYNTHESIS AND STRUCTUREAL CHARACTERIZATION OF ENHANCED TIO$_2$-GO STRUCTURES

The influence of the synthesis methods and conditions on the morphology and chemical properties of TiO$_2$-GO photocatalyst is discussed. In this chapter, the GO loading and the heat treatment are compared and discussed in term of morphology, chemical and thermal properties.

3.1. SYNTHESIS OF TiO$_2$-GO

Over the past years, the synthesis of TiO$_2$-graphene oxide composites by both physical mixing and chemical reaction routes has been investigated with the aim to obtain excellent photocatalytic property. Comparing with the mixing process, the chemical reaction gives stronger interaction between TiO$_2$ and graphene oxide. Via the chemical reaction route, the moiety functional groups on graphene oxide act as nucleation sites for the growth of TiO$_2$ nanocrystals [21–23]. Methods involving the *in-situ* nucleation and growth allow obtaining interface bonding between the two materials. In addition, by controlling pH of the reaction medium, it is possible to realize strong electrostatic interaction between the positive charge surface of TiO$_2$ particles and the negative charge surface on graphene oxide sheets [20,24]. In general, appropriate pH is around 4-7 [23,24]. In addition, post-synthesis thermal treatments promote formation Ti-O-C and/or Ti-C interface bonding, increase TiO$_2$ crystallinity, and cause the partial reduction of graphene oxide [18,19]. The benefit of these structural feature characteristics is an improved electrons transfer via interface bonding from TiO$_2$ to graphene and therefore an enhanced photocatalytic activity [2,16]. Moreover, the synergistic interaction of TiO$_2$ and graphene oxide can narrow the ban gap of the photocatalyts, resulting in a better exploitation of the solar light [8,15]. Furthermore, the ratio of graphene oxide and TiO$_2$ can strongly influence the photocatalytic activity, since high amount of graphene oxide can shield TiO$_2$ photocatalytic particle from light excitation, thus decreasing their photocatalytic activity [16,26,27].

As mentioned in Chapter 2 above, in this thesis the sol-gel method was used for TiO$_2$-GO synthesis. In addition, the pH is controlled at pH 6 due the electrostatic interaction. A TiCl$_4$ solution was added to a GO suspension in an ice bath (~2±1°C) and stirred to obtain a cold homogenous dispersion. After removing the ice bath, NH$_4$OH was added to the suspension to reach pH 6, thus promoting electrostatic

interaction between the two materials. The suspension was then heated for 4 hours up to 100 °C in a stirred flask (dynamic method, TD and GTD samples) or hydrothermally treated between 100 and 200°C in static tank (static method, TS and GTS samples). The TiO$_2$-GO (GT) syntheses are discussed in Paper I and Paper III. The synthesis strategy adopted in this thesis is showed in Figure 3-1.
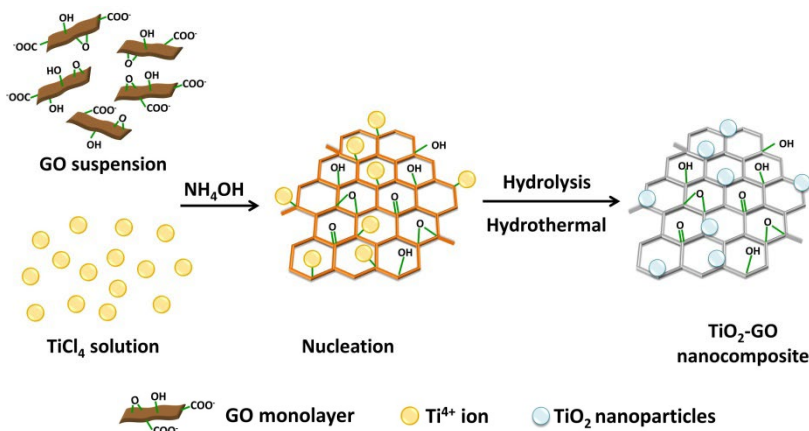
Figure 3-1 Schematic of TiO$_2$-GO nanocomposites synthesis.

To study the effect of the incorporation of GO on the morphology and photocatalytic properties of the TiO$_2$ nanoparticles, GO was loaded up to 50% (50GTD) in the composites. The effect of the reaction time on the morphologies of GT composites was observed by comparing samples prepared at 4 and 24 hours for 1wt% GO loading. In addition, at this concentration of GO the effect of stirring during synthesis (dynamic and static method) was also investigated. Herein, the GO-TiO$_2$ nanocomposites are named GTD and GTS for the dynamic and hydrothermal (static) synthesis methods, respectively. The number in front of those letter represent the weight of GO (%), and the numbers after is the temperature of the synthesis.

3.2. TiO$_2$-GO NANOMATERIALS

To understanding the effects of TiO$_2$-GO interlinkage bond and GO structure evolution during heat treatment, GO and TiO$_2$ were synthesized at the ratio 1:1 (50GTD) and hydrolysis from 60-100°C. The morphology and the thermal behavior are presented in this part.

3.2.1. MORPHOLOGIES OF TiO$_2$-GO NANOMATERIALS

The three micrographs in Figure 3-2 illustrate the microstructures of 50GTD-100. The SEM image in Figure 3-2a exhibits packed TiO$_2$ nanoparticles with a few

nanometer sizes, but unfortunately GO sheets cannot be observed from this picture. On the contrary, the HR-TEM image (Figure 3-2b) reveals that GO sheets are partly covered with agglomerated TiO_2 nanoparticles and can from thin GO nanoribbons (red arrows). Figure 3-2c shows the characteristic structures of GO (red arrows) and TiO_2 crystals (black arrows). The restacking of GO layer is a typical structure because of the van der Waals interactions and hydrogen bonding [98]. In addition, the TiO_2 anchoring over GO ribbons is clearly seen in the red circle.
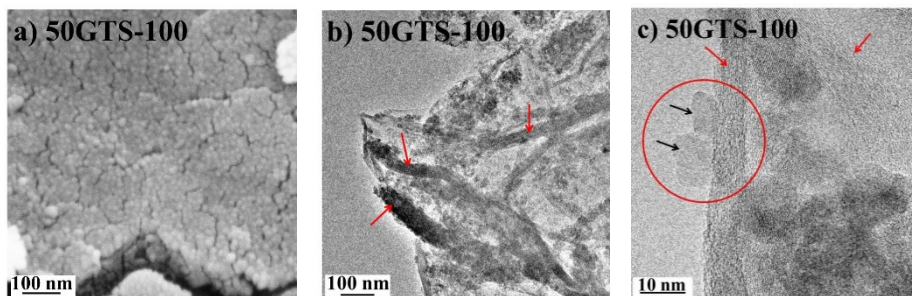
Figure 3-2 The microstructure photos of 50GTD-100 are taken by a) SEM, b) and c) HRTEM with low and high magnification, respectively. The red arrows point at GO, the black arrows point at TiO_2 nanoparticles and the red circle is anchoring TiO_2 nanocrystal over GO. The Figures reproduced from Paper I with the permission from the Royal Society of Chemistry.

Figure 3-3a shows the characteristic XRD peaks of both GO and TiO_2 in 50GT composites synthetized at different temperatures and of a pure TiO_2 reference. It is found that the GO peak in all of composites occurs at $2\theta = 11\text{-}12°$, which is a higher angle than for the starting GO ($2\theta = 10.46$). The typical peak of GO allows to calculate the interlayer distance and domain (ribbon) thickness of GO through the Bragg law and the Scherrer equation, respectively. The results of these calculations are shown in Figure 3-3b. The staring GO has *d*-space of 8.45 Å and average thickness of the GO ribbons is 24 nm. During synthesis, GO is exposed to heat and its functional groups can interact with the forming TiO_2 clusters. Under this conditions, even if the temperature of the reaction mixture does not exceed 100°C, GO can undergo partial reduction. As a consequence , we can observe a small decrease of the *d*-space distance, which is ~ 8.1 Å for all the samples except the one synthetized at 100°C, for which is 7.36 Å. The presence of the TiO_2 nanoparticles and the partial reduction of GO caused also a less efficient stacking of the GO layers, as it can be observed from the GO ribbon thickness measured by the Scherrer equation [99].

The characteristic peaks of TiO_2 (Figure 3-3a) can be observed both in the composites and pure TiO_2 reference. Higher is the synthesis temperature, higher the crystallinity of TiO_2 in GTD composites (the anatase main peaks can be observed only for powders synthetized ≥ 70°C, and brookite arise in simple synthetized ≥

80°C). The plot between crystal size and the weight fraction of anatase, and the synthesis temperatures is in Figure 3-3c. The crystal size of anatase in the composites increases with temperature reaching 6.4 nm for 50GTD-100, while the pure TiO_2 reference, TD-100, has size of about 7.5 nm. This result shows that GO limits the growth of TiO_2 crystal. In addition, the anatase fraction of TD-100 and 50GTD-100 is slightly above 70%.
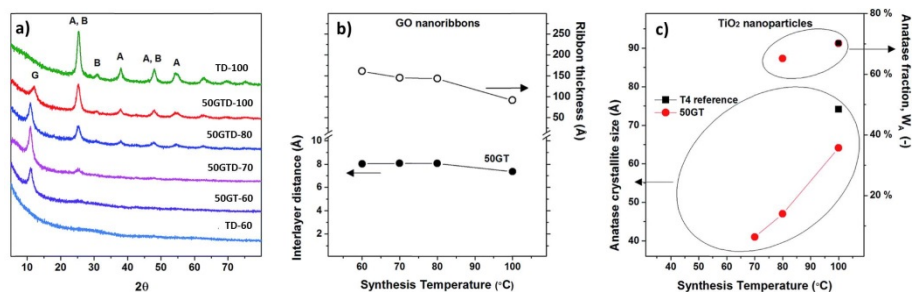
Figure 3-3 a) XRD patterns of 50GTD composites and TD prepared at 60-100°C for 4 hours; G represents the characteristic graphene oxide peak, A and B stand for anatase and brookite peaks, respectively. b) Plot of GO interlayer distance and domain (ribbon) thickness in GT composites as a function of the temperature. c) Crystal size and fraction of anatase as a function of the synthesis temperatures. The Figures are reproduced from Paper I with the permission from the Royal Society of Chemistry.

3.2.2. FUNCTIONAL GROUPS OF TIO$_2$-GO NANOMATERIALS

The chemical evolution of GO functional groups during synthesis and the interface bonding between TiO_2 and GO are discussed in this paragraph. The FT-IR analysis (Figure 3-4a) of pure TiO_2 shows a well pronounced peak below 800 cm^{-1}, which corresponds to the Ti-O-Ti vibration, and 2 small peaks, which can be assigned to Ti-O stretching and O-H vibration at 1385 and 1630 cm^{-1}, respectively [100]. The starting GO presents the complex system of peaks, which is described in section 2.1.2. The spectrum of the mixed 50GTD-100 sample shows the peaks corresponding to its component TD-100 and GO. However, the peaks in the interval 855-1731 cm^{-1} have the lower intensity than those in the spectrum of the pure GO sample. This can arise from the lower GO concentration and from the partial reduction of GO during synthesis. In addition, the broaden peak at around 400-750 cm^{-1} indicates the presence of both Ti-O-Ti and Ti-O-C bonds. Indeed, it was explained that functional groups on GO and hydroxyl group of TiO_2 can form the Ti-O-C bonding by condensation [101].

Figure 3-4b shows the binding energy of the C1s electrons in GO and 50GTD-100. As explained above (paragraph 2.1.2), the curve of GO, can be deconvoluted in three main peaks corresponding to aromatic C, C-O and O-C=O groups at 284.6, 286.5

and 287.7 eV, respectively. In 50GT-100, these three peaks are centered the same position of pure GO, but their relative areas change. Partial reduction on GO in the composite is studied by calculating the area ratio between the oxidizing carbon and the reduced carbon atoms: A_{C-O}/A_{C-C} and $A_{O-C=O}/A_{C-C}$ [100]. It is found that for GO, the A_{C-O}/A_{C-C} and $A_{O-C=O}/A_{C-C}$ are 1.34 and 0.41 eV, respectively. On the contrary, 50GTD-100 has $A_{C-O}/A_{C-C} = 0.65$ and $A_{O-C=O}/A_{C-C} = 0.26$. Therefore, the area ratios of the oxidized peaks decline of about 50% comparing with starting GO. This suggests that nearly half of the functional moieties of GO is removed after *in-situ* nucleation and growth of TiO_2 at 100°C. The deconvolution of the O1s peaks is reported in Figure 3-4c. The pure TiO_2 sample, TD-100, presents two peaks at 529.8 eV (Ti-O-Ti) and 530.5 eV (Ti-OH) [102]. The GO curve can be deconvoluted into three sub-peaks, as discussed in Paragraph 2.1.2. Meanwhile, 50GT-100 shows the characteristic peaks of the two materials [103].
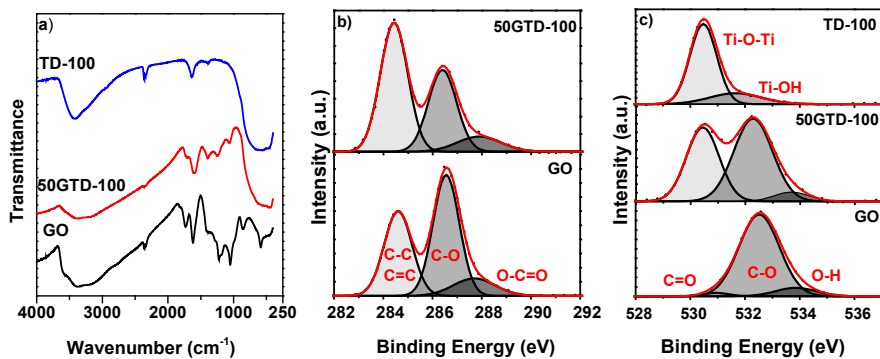
Figure 3-4 a) FTIR transmittance spectra and XPS spectra of b) C1s and c) O1s of GO, 50GTD-100 and TD-100. The XPS results (dotted black line) are fitted with the component peaks (grey area) resulting the fit spectra (red).

3.2.3. THERMAL PROPERTIES OF TIO$_2$-GO NANOMATERIALS

DSC analysis was conducted to study the thermal transition behavior of GO, TiO_2 and 50TGD composites. The DSC curves of the nanomaterials are shown in Figure 3-5a. Regarding the pure GO curve, the exothermic peak caused by the decomposition of its functional groups has onset at 149°C ($T_{GO,onset}$) and mimium at 187°C ($T_{GO,min}$). All of the composites have the same characteristic peak GO, but both $T_{GO,onset}$ (over 180°C) and $T_{GO,min}$ (over 190°C) occur at higher temperatures. This suggests that TiO_2 nanoparticles have a strong interaction with GO and can retard the degradation of GO functional groups. Figure 3-5b shows the difference in onset temperature ($\Delta T_{GO,onset}$) between composites and the starting GO as a function of the synthesis temperature. $\Delta T_{GO,onset}$ decreases when the temperature of synthesis increases. This can be explained by considering that TiO_2 nanoparticles prepared at

low temperatures are highly amorphous and have small size, thus they are more reactive and have high specific surface area to interact with GO [97].

The phase transitions of TiO_2 can be observed in Figure 3-5c, as detected by DSC. The TiO_2 prepared at 60°C is transformed from amorphous to anatase and anatase to rutile at 470°C and 570°C, respectively [104]; whereas TiO_2 synthetized at 100°C shows only the anatase-to-rutile transition (570°C). The GTD-60 is similar to TD-60 but the transformation shifted higher around 10°C. Indicating that GO has still some interaction with the oxide material, even after been exposed at high temperature and therefore reduced. The GTD composites synthesized from 70-100°C show a small peak of the anatase to rutile phase transformation at 570°C.
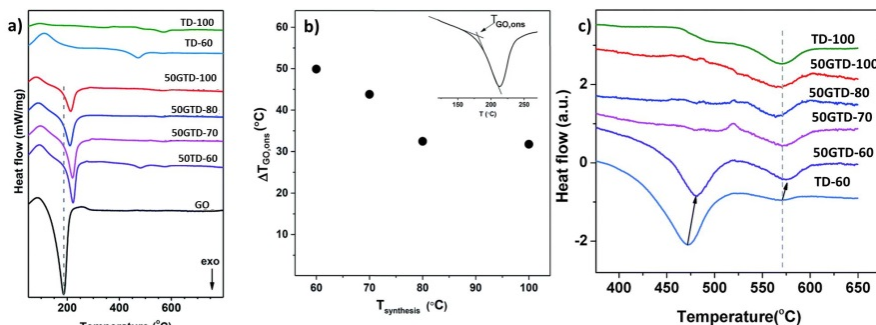
Figure 3-5 a) DSC curves of GO, pure TiO_2 (TD-60 and TD-100 and 50 GTD composites synthesized from 60-100°C. b) The different of the on-set reduction temperatures ($\Delta T_{GO,onset}$) between the 50GTD composites and GO with the temperature of hydrolysis synthesized. c) The DSC curves from 400°C to 650°C of TiO_2 transition temperature for TD and 50GTD synthesized in deferent temperature. The Figures reproduced from Paper I with the permission from the Royal Society of Chemistry.

3.3. SYNTHESIS OF TIO$_2$-GO WITH ENHANCED BONDING

This section presents the morphology and chemical structure of the enhanced TiO_2-GO nanomaterials, since there are many factors influencing their properties. First of all, the effect of the GO loading and reaction time on the structural order/disorder in TiO_2-GO heteromaterials is studied. Secondly, two types of preparation methods, dynamic and static, are compared on the base of the morphology and the functionalities of the materials. Lastly, the high temperature of static synthesis (hydrothermal) is conducted to study the reduction of GO and the chemical interface between GO and TiO_2.

3.3.1. MORPHOLOGIES OF TIO$_2$-GO WITH ENHANCED BONDING

3.3.1.1 ORDER/DISORDER STRUCTURE

The Pure TiO$_2$ (TD-100) and 1GTD-100 microstructures are shown in Figure 3-6. The TiO$_2$ nanoparticles of the two materials have similar aggregation, particle size and shape, consistently with the low GO loading in 1GTD-100. Figure 3-6a and 3-6c show that both TD-100 and 1GTD-100 consist of agglomerated TiO$_2$ nanoparticles with diameter of about 10 nm. In addition, the fringe pattern analysis of the high magnification image of TD-100 (Figure 3-6b) reveals an interplane distance of 0.35 nm, corresponding to the (101) plane of anatase. Moreover, 1GTD-100 shows the presence of a single GO layer, on which TiO$_2$ nanoparticles are anchored (red Figure 2-6c and 2-6d). Contrary to the micrograph of the 50GTS-100 sample in Figure 3-b, 1GTD-100 has no nanoribbon structures. On the contrary, GO is present as isolated wrinkled sheet. In this case, the very low GO loading caused GO sheet to be covered/intercalated with TiO$_2$ particles and therefore prevented their stacking in nanoribbons.

Figure 3-6 HR-TEM micrographs of TD-100 and 1GTD-100: low and high magnification in the first and the second row, respectively. The red arrows point at GO and the red circle indicate a TiO$_2$ nanocrystal anchored over GO. The Figures reproduced from Paper II.

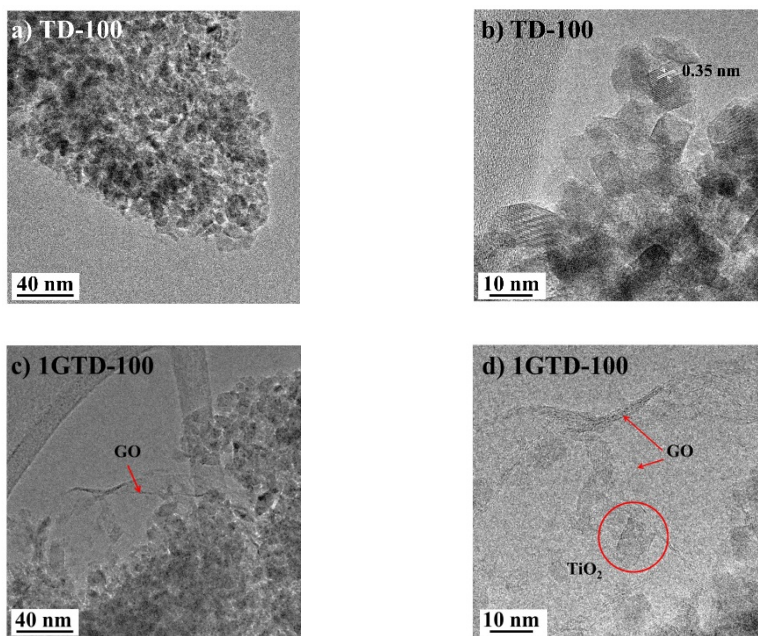The XRD pattern of GO, TD-100, 1GTD-100, 1GTD-100(24), and 50GTD-100 is plotted in Figure 3-7a). The sample 1GTD-100(24) was prepared under the same condition of 1GTD-100, but let to react for 24 hours instead of 4 hours. 1GTD-100 and 1GTD-100(24) do not show the characteristic GO peak due to the low concentration of GO [40,105]. TiO_2 in all samples consists of both anatase (A) and brookite (B) phases. The anatase weight fraction is slightly higher than 70% in all the samples. The FWHM of characteristic peak at 2θ =25.2° is used for calculating anatase crystallite size, resulting in 6.4, 6.6, 8.3 and 7.5 nm for 50GTD-100, 1GTD-100, 1GTD-100(24) and TD-100, respectively. In addition, SAXS analysis (Figure 3-6b) reveals the size distribution of TiO_2 nanoparticles in TD-100 and TGD-100 composites. SAXS results shows slightly bigger values than those calculated from Scherrer's equation from XRD diffractogram. However, both of analysis techniques shows the same trend and confirms that TiO_2 crystals have size smaller than 10 nm diameter, both in pure titania and in GTD composites prepared at 100°C. Moreover, both measurements indicate that the loading of GO in the GTD composites, results in TiO_2 particle with a smaller size than those of the pure titania reference sample. This can be explained considering that the oxygen functional groups on graphene oxide act as nucleation sites for Ti^{4+} and titania cluster growth during synthesis [21–23]. Moreover, TiO_2 crystal size is not affected by the GO loading (1 and 50 wt%), since the concentration of nucleation sites in 50GTD-100 is reduced from the GO stacking nanoribbon structures. Moreover, as expected, the size of TiO_2 particles increases with the synthesis time.
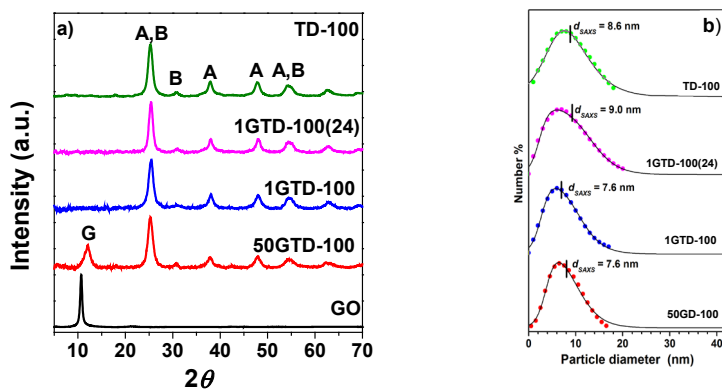
Figure 3-7 a) XRD patterns of starting GO, TiO_2 and GTD composites with 1and 50 wt% GO prepared with hydrolysis at 100°C for 4 hours (1GTD-100 and 50GTD-100, respectively), and 1GTD-100 preparing at 24 hours (1GTD-100(24). b) Particle size distribution of TiO_2 in TD and GTD composites was analyzed with SAXS technique. The dots indicate the Dv(R) distribution functions and the lines correspond to the Log-normal distributions. The average particle diameters, d_{SAXS}, were calculated from the Dv(R) distribution functions. The Figure b) is reproduced from Paper I with the permission from the Royal Society of Chemistry.

3.3.1.2 PREPARATION METHODS AND RATIO OF GO: TIO$_2$

The structural configuration of pure TiO$_2$ and GT composites with different preparation methods (static and dynamic) is investigated by TEM. TS-100, Figure 3-8a, consists of highly agglomerated of 10-12 nm large TiO$_2$ nanocrystal with polyhedral shape. The study of the fringe patterns indicates the (101) plane of anatase phase with 0.35 nm *d*-spacing. The (111) plane corresponding to brookite patterns with the 0.346 nm *d*-spacing could not be excluded. In addition, TiO$_2$ nanoparticles in both composites, namely 1GTS-100 and 1GTD-100 (Figure 3-8a – 3-8f), have morphology similar to TS-100 and TD-100. Due to the very low amount of GO, GO monolayers are rarely observed in the TEM micrographs of the composites, as clarified in 3.1.1. Fortunately, a GO monolayer is visible in the micrographs of 1GTD-100, and it is indicated with red arrows in Figure 3-8e and 3-8f.
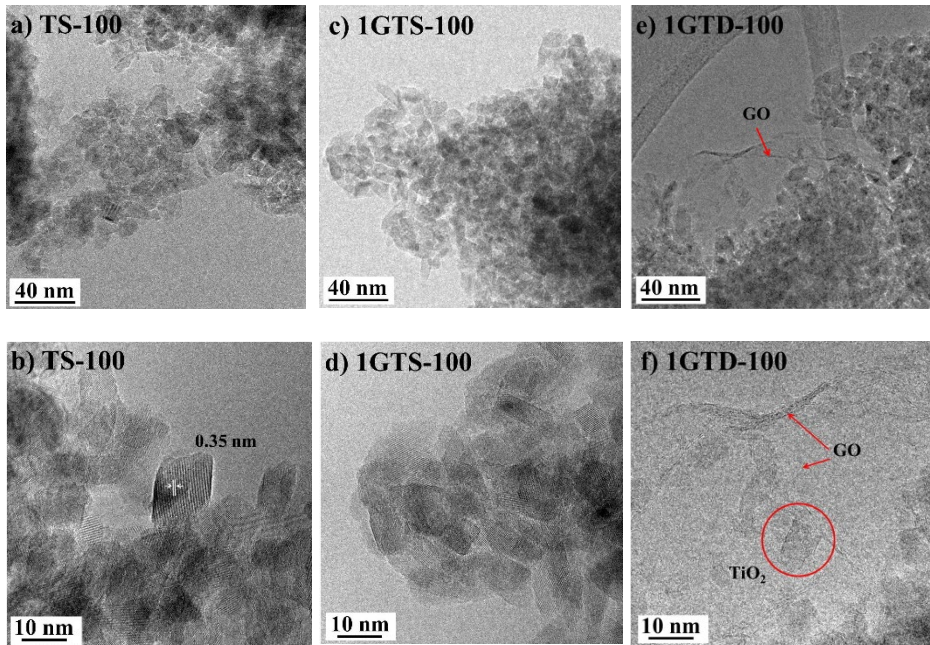
Figure 3-8 HRTEM figures of pure TiO$_2$ (TS-100) and 1GT composites prepared under static (1GTS) and dynamic (1GTD) conditions were taken with low (first row) and high magnification (second row), respectively. The red arrows point at a GO sheet and the red circle indicates a TiO$_2$ nanocrystal over GO. Figures are taken from Paper II.

The phase compositions study of TiO$_2$ in TS-100 (synthesized TiO$_2$) and GT composites prepared in different reactors and different weight ratio (0, 0.05, 0.1, and 1 wt%) of GO are displayed in Figure 3-9a and Appendix A. GO has its

characteristic peak at $2\theta = 10.46°$. Such peak is not present in the GT composites due to the low graphene oxide concentration. The XRD diffractograms of TS-100 and GT-100 reveal that they are a mixture of anatase and brookite. The weight ration of these two phases is calculated using the peak at $2\theta = 25.2$ of anatase TiO_2 and shows approximately 77% anatase in pure TS-100. This value is close to the number obtained from TD-100, 0.05GTD-100 and 1GTD-100 synthesized in the stirred Pyrex reactor (approximately 75% anatase). On the other hand, TGS-100 composites appear to have a slightly higher amount of anatase; approximately 77-79%. Unfortunately, the fraction number of anatase could not express in exact number due to the systematic error and the bias from fitting peak procedure. In conclusion, the difference of anatase fraction from both dynamic and static reactors (stirring in Pyrex beaker and no stirring Teflon vessel, respectively) could be negligible.

The particle size distribution of TiO_2 of GO loading 0-1wt% calculated from XRD peak obtained by the static condition and the dynamic synthesis are 8 nm and 7.5 nm, respectively. The SAXS analysis indicates 8-9 nm average size of TiO_2 from both conditions.
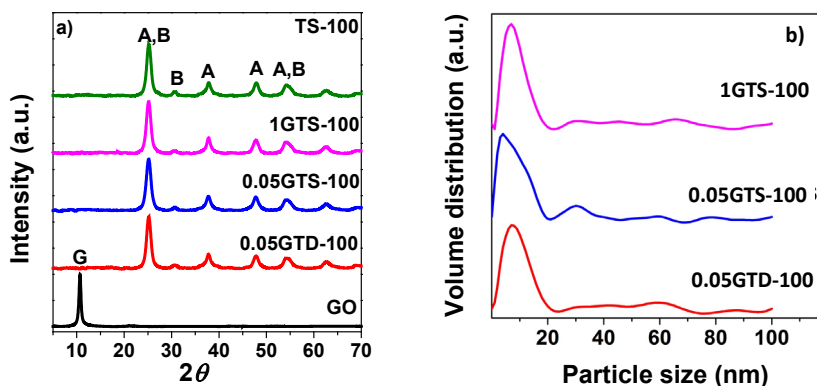
Figure 3-9 a) XRD patterns of starting GO, TiO₂ (TS-100) and GTS composites with 0.05 and 1 wt% GO prepared with static (0.05GTS-100 and 1GTS-100, respectively) and dynamic (0.05GTD-100) conditions at 100°C. G represents graphene oxide peak, A and B stands for annatase and brookite peaks, respectively. b) Particle size distribution of TiO₂ in GT composites by SAXS analysis. Figures are taken from Paper II.

3.3.1.3 HIGH TEMPERATURE TREATMENT

The morphology of 0.05GTS nanocomposites prepared by hydrothermal treatment from 100-200°C is studied via TEM images in Figures 3-10. All pictures reveal that the GTS composites consist of both graphene oxide or reduced graphene oxide (red arrows, Gr) and TiO_2 nanoparticles (black arrows). In addition, the lattice analysis of 1GTD in Figure 3-10d reveals a *d*-spacing of 0.35 nm, corresponding to the (101)

anatase plane, but also to the (111) bookite plane (0.346 nm). The TiO_2 nanocrystals have the same morphology in all conditions of synthesis: highly aggregated, with polyhedral shape, and with size of around 10-15 nm.
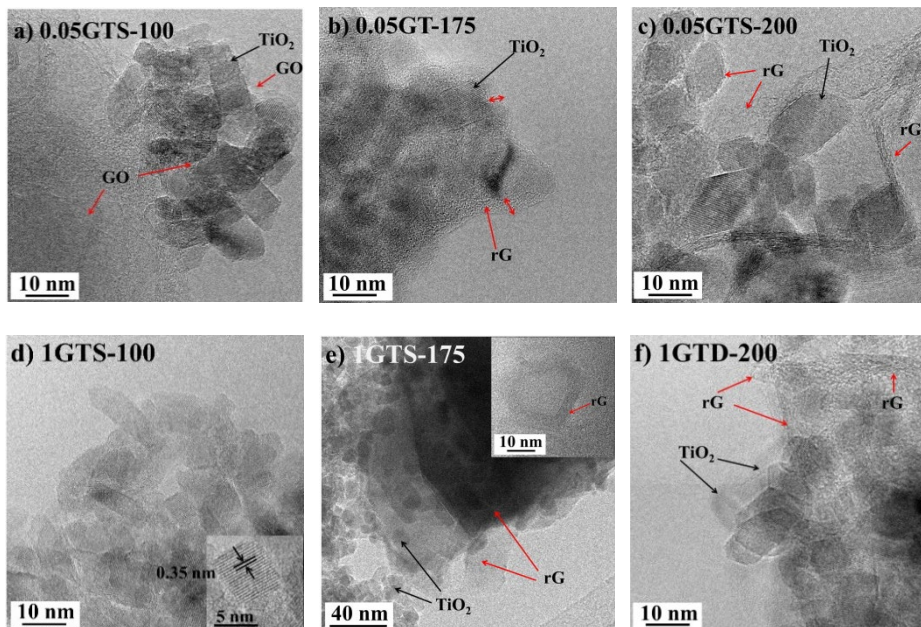
Figure 3-10 HRTEM pictures of 0.05GTS and 1GTS synthesis with hydrothermal method from 100-200°C were taken at high magnification. The red arrows point at GO, the black arrows point at TiO_2 nanoparticles and the white dotted line is stacking GO. Figures are taken from Paper III.

Graphene oxide undergoes thermal reduction in the range of temperatures between 100 and 200°C. During reduction, it can interact with TiO_2 nanoparticels, thus changing it morphology depending on the synthesis temperature. At low temperature (100°C), TiO_2 nanocrystals lay on GO or fully cover GO planes (Figure 3-10a and 3-10d, red arrow). In Figure 3-10a, we can observe also structures arising from the restacking of a few layers GO nanoribbon. Increasing the synthesis temperature to 175°C, GO is partially reduced and prefers to form stacked structures (due to the van der Waals interactions [106]). Moreover, these reduced GO ribbons together with amorphous carbon layers (rG, red arrow), which have thickness of about 3.8 – 5 nm, can wrap TiO_2 nanoparticles, as we can observe for 0.05GTS-175 in Figure 3-10b. However, 1GTD-175 (Figure 3-10e), which contains more GO than 0.05GTS-175, shows both reduced GO plates intercalating TiO_2 nanoparticles and onion-like structures of multilayer reduced graphene oxide (picture inset). The formation of these shell-structures was ascribed to the reconstruction and recombination of dandling bond on carbon atoms forming π-bond during reduction [107]. Such rGO

shell can be unfolded due to fast releasing of gas products from the functional groups on GO [108]. Hence, it is possible to find winkled graphene sheets or graphene nanoribbons in GTS-200 (Figures 3-10c and 3-10f). In addition, we can also observe TiO_2 nanocrystals enclosed with < 1 nm thin amorphous carbon layers.

Because of the very low amount of GO loading, graphene materials in GTS composites are not detected by XRD analysis in Figure 3-11. Actually, peaks of graphene oxide (G) and reduced graphene oxide (rG) should arise around $2\theta = 10.46$ and $2\theta = 23.9$, respectively. In addition, the TiO_2 phase composition in the GTS composites is still the same such the anatase mixed with brookite but in different weight fraction. The amount of anatase increases with synthesis temperature from 80 to 85 and to 92% in samples synthesized at 100, 175 and 200°C, respectively, for both TS and GTS nanocomposites. In addition, TiO_2 crystal has sizes of 8, 11 and 13 nm for TS and GTS samples synthetized at 100, 175 and 200°C, respectively.
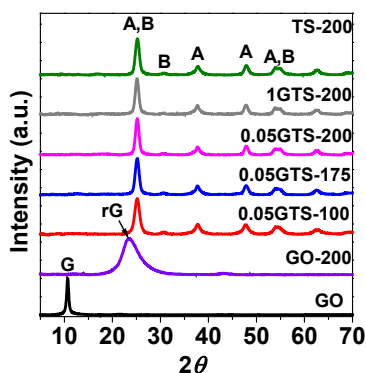
Figure 3-11 a) XRD patterns of starting GO, GO-200, TiO_2 (TS-100) and GTS composites with 0.05 and 1 wt% GO prepared with static (0.05GTS-100 and 1GTS-100, respectively) and dynamic (0.05GTD-100) conditions at 100°C. G represents graphene oxide peak, rG is reduced GO, A and B stand for anatase and brookite peaks, respectively.

3.3.2. FUNCTIONAL GROUPS OF ENHANCED TIO₂-GO

Functional groups in TiO_2-GO materials and the degree of reduction on GO were investigated by XPS analysis. The deconlvolution technique was used to extract the peak components (grey peaks in Figure 3-12). C1s spectra of GO and 1GTD-100 is divided in 3 main peaks, as showed in Figure 3-12a. GO has the non-oxidizing (C-C/C=C) carbon peak at biding energy of 284.6 eV and 2 peaks of oxidized carbon atoms, namely C-O and C=O/O-C=O, with binding energy at 286.5 and 287.7 eV, respectively [109]. All 1TG-100 composites have 3 main peaks for the C-C/C=C peak and C-O peak with the similar binding energy of GO, while the C=O/O-C=O peak moves from 287.7 to 289.1-189.3 eV, due to the formation of Ti-O-C bonds

[25,110]. In addition, the deconvolution peak at binding energy around 532 eV (O1s, Figure 3-12b) of 1GT-100 confirms the presence of Ti-O-C bond. This characteristic peak is present also in the spectra of 1GTD-100 and 1GTD-100(24), 1GTD-100 and 1GTS-100, that is, in sample prepared with different synthesis method and synthesis durations. Indeed, the formation of Ti-O-C bond has been explained to the relocation of C-O and COOH due to lower stability during the hybridization process with TiO_2 and converts to in-plain epoxy [102,111]. Others 2 main peaks in 1GT-100 composites imply the vibration mode of Ti-O-Ti at 530.5 eV and of –OH at 533.5 eV [16,102]. Unfortunately, it was not possible to detect the signals from GO loadings lower than 1wt% due to the higher background intensity from the ubiquitous carbon contamination [112].
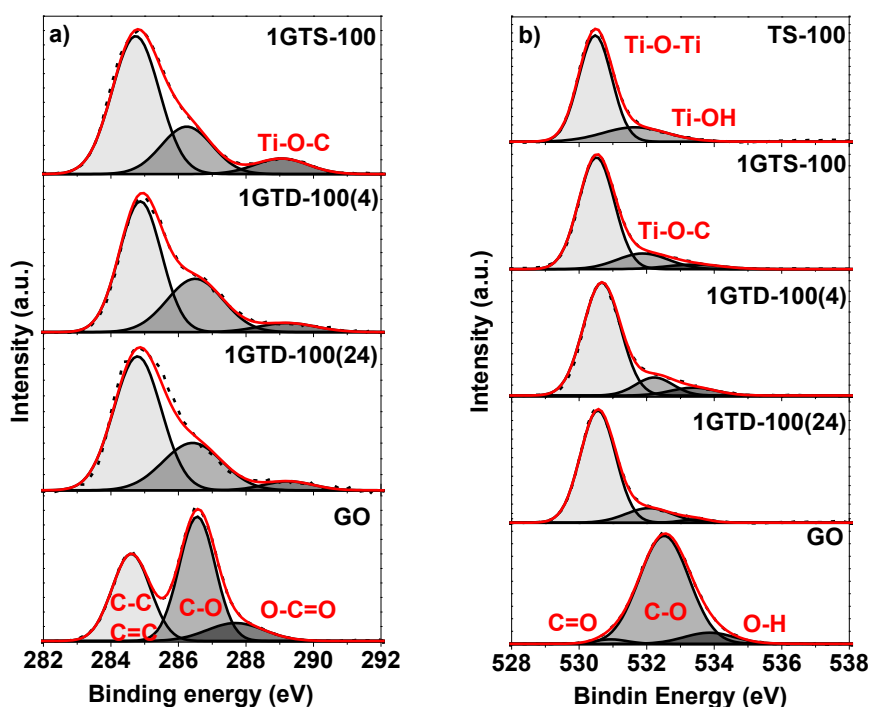
Figure 3-12 XPS spectra of a) C1s and b) O1s of GO, GT composites prepared at 100°C in statistic and dynamic reactors. The dotted black lines is fitted with the component peaks (grey area) resulting the fit spectra (red).

The formation of Ti-O-C bond in TG composites is an important structural feature, that may promote the electron transfer from TiO_2 to graphene oxide and thus enhance the photocatalytic performances of the nanocomposites [16]. The Ti-O-C linkage (289.1 eV) was also found in 1TGS composites synthesized via hydrothermal (static) process from 100-200℃ as shown in Figure 3-13. In addition,

Ti-C (blue peak) bond is present in the 1GTS composites prepared at 175 and 200°C. Indeed, the deconvolution of C1s peaks indicate the C-Ti bond at binding energy 283.85 eV and 2 peaks of C-C/C=C at 285 and C-O at 286.5 eV [113,114]. Both Ti-O-C and C-Ti bonds promote more the photocatalytic activity since both of the interface bonding support the electron transfer [91,115].
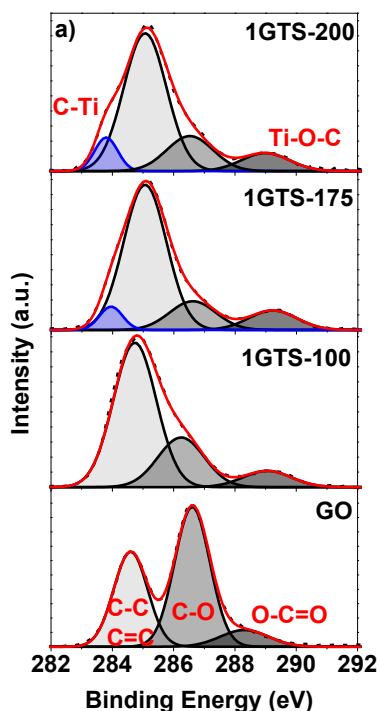
Figure 3-13 XPS spectra of C1s and of GO, GTS composites prepared via in-situ hydrothermal process. The dotted black line is fitted with the component peaks (grey and blue area) resulted the fit spectra (red). Figure is taken from Paper III.

The degree of the partial reduction of graphene oxide in both starting GO and GT composites was measured from the XPS C1s peak area ratio as explained in 3.2.2. The values of A_{C-O}/A_{C-C} and $_{AO-C=O}/A_{C-C}$ are presented in Table 3-1. In general, graphene oxide in all GT composites presents a lower degree of oxidation, when compared to the starting GO. The reduction of graphene oxide can be explain by two reasons: i) the oxygen functional groups act as nucleation sites for Ti^{4+} and donate oxygen for TiO_2 growth; ii) oxygen functional groups degrades due to the heating during synthesis, as explained in 2.1.3. Partial reduction of GO is desired, as it can improve the electron acceptor properties of GO [98,116] for a better synergy with the photocatalytic TiO_2 center

Table 3-1 XPS peak area ratio (A_{C-O}/A_{C-C} and $A_{O-C=O}/A_{C-C}$) of GO and GTD and GTS composites

Sample name	A_{C-O}/A_{C-C}	A_{O-C-O}/A_{C-C}
GO	1.34	0.41
50GTD-100	0.65	0.26
1GTD-100(4)	0.54	0.27
1GTD-100(24)	0.44	0.28
1GTS-100	0.65	0.24
1GTS-175	0.19	0.14
1GTS-200	0.24	0.13

3.4. Summary

In order to design GT composites for photocatalytic applications, it is important to understand interactions and evolution of GO and TiO_2 during synthesis and thermal annealing. GT composites with 50 wt% GO loading were prepared to study the structural evolution of the material. They consisted of anatase-brookite TiO_2 nanoparticles with polyhedral shape laying on GO monolayers or decoration GO nanoribbons. The size and the anatase fraction TiO_2 particles increase with increasing the synthesis temperature, while GO gets partially reduced. The interaction between TiO_2 particles and GO is confirmed by FTIR and XPS results, showing Ti-O-C bonding. This strong interaction is confirmed by the TEM micrographs of the samples, showing facets of TiO_2 nanoparticles over GO nanoribbon. This interface bonding between GO and TiO_2 is strong enough to retard the phase transformation during thermal annealing.

TiO_2-GO materials prepared at GO loadings $\leq$ 1 wt% resulted in highly agglomerated anatase-brookite nanocrystals laying on single layers of GO. The preparation method (static vs dynamic) had little influence on the morphology of the materials. The size of TiO_2 nanoparticle became bigger, when the reaction time was increased to 24 hours but the anatase fraction did not change.

XRD analysis and TEM pictures gave no evidence of GO nanoribbons in samples synthetized at 100 °C with GO loading $\leq$ 1%, indicating that in these samples GO layers are interacted with TiO_2. However, increasing the synthesis temperature to

175°C, the structure of GO is partly reduced and prefers to restack and form 3.8-5 nm thick layers of amorphous carbon or onion-like rGO structures, wrapping TiO_2 nanoparticles. When the synthesis temperature reach 200°C, GO is further reduced. Under these circumstances, the close shell rGO structures might eventually re-open and multilayered rGO ribbons are found in the TEM images of 0.05GT-200. In this sample, some of the TiO_2 particles are partially coated by amorphous carbon. However, such amorous carbon layer is thinner than 1 nm.

The XPS analysis revealed that different kinds of interface bonding can be established depending on the synthesis temperatures. The Ti-O-C bonding was observed in all the samples, while Ti-C bonding was present only in material synthetized at a temperature ≥ 175°C. In addition, the degree of reduction on GO depends on the synthesis temperature. Half of the functional groups on GO was eliminated during synthesis at 100°C, but GO was reduced to a much larger extent when synthesis was performed at T ≥ 175°C. Future more, the reduction of GO do not depend on the GO concentration and the synthesis time (4 or 24 hours).

The next chapter deals with how these structural features can influence the photocatalytic performances of TiO_2-GO composites.

CHAPTER 4.

PHOTOCATALYTIC PROPERTY OF TIO$_2$-GO MATERIALS

In this chapter, the light reflection and the band gap energy of the synthesized TiO$_2$-GO materials are presented since these features have a great impact on photocatalytic activity. The potential of TiO$_2$-GO photocatalytic materials is reported in term of the phenol degradation under simulated sunlight and discussed based on the material morphology.

4.1. OPTICAL PROPERTIES OF TIO$_2$-GO MATERIALS

The study of the UV-Vis light diffuse reflectance is here conducted to describe the electronic behavior of the semiconductor materials and to estimate their absorption edge [117]. Diffuse reflectance spectra were taken with an integration sphere, using BaSO$_4$ as the reference material. The plot of diffuse reflectance spectra of GT-100 and TS-100 are shown in Figure 4-1a.
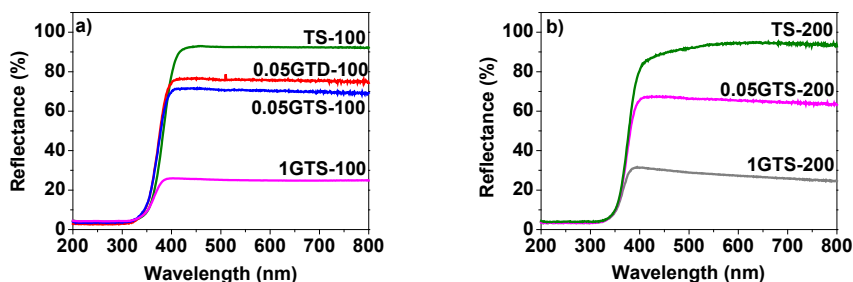
Figure 4-1 The diffuse VU-Vis spectra of Pure TiO$_2$ and GT composites preparing in different ratio of GO loading. a) The spectrum of TS and GT composites prepared with static and dynamic reactors at 100°C and b) TS and GTS composites prepared with hydrothermal treatment at 200°C. The Figures a) is taken from Paper II.

TS-100 has the lowest absorption (Reflectance about 95%) for wavelengths higher than 400 nm. The spectra of the GT composites show the same shape and similar adsorption edge, but they have a higher light absorption above 400 nm. The absorption of GT composites increases with amount of GO loading: 30% absorption for 0.05GTS-100 and 75% absorption for 1GTS-100, approximately. This can be explained by the fact that GO is dark and acts as light absorber. Surprisingly, the absorption spectra of TS and GTS samples prepared at 200°C are similar to those of

the corresponding samples obtained at 100°C composites. Hence, the absorption of GT composites depends on the GO loading. The absorption edge of all composites is only slightly red-shifted compared to TS reference.

The band gap energy (E_g) of the photocatalytic materials was obtained from Tauc's equation (4-1) [118].

$$(\alpha h v)^{1/2} = C(h v - Eg) \qquad\qquad 4-1$$

where α is the absorption coefficient of the solid , $\frac{(1-R)^2}{2R}$, R is the reflectance [119], at a certain wavelength *(λ)*, *h* is Planck's constant (4.136 ×10^{-15} eV s), *C is* a proportionality constant, and v is the frequency of light obtained by dividing the speed of light (c = 3×10^8 m.s^{-1}) for the wavelength. The band gap energy can be estimated by extrapolation from the relationship plot between $(\alpha h v)^{1/2}$ and the photon energy $\frac{1239}{\lambda}$ [118,119] in Figure 4-2a. The band gap energy is 3.3 eV for pure TiO$_2$ and 3.2 eV for the GT composites, irrespective of the synthesis method and of the GO loading. The Tauc plot for pure TiO$_2$ and GTS composites synthesized at 200°C is shown in Figure 4-2b. The band gap energy of these semiconductors ranges from 3.28 eV for TS-200 and 3.32 eV for 1GTS-200 and therefore, it is similar to that of the materials prepared at 100°C.
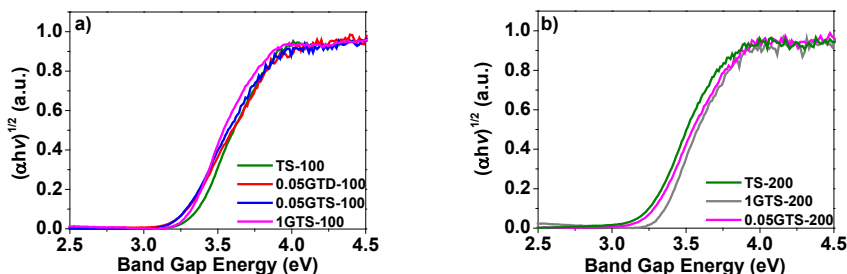
Figure 4-2 The plot of $(\alpha h v)^{1/2}$ against gap energy of Pure TiO$_2$ and GT composites preparing in different GO loading ratio with a) the stirring and without stirring vessels at 100°C and b) the hydrothermal method at from 200°C. The Figure a) is taken from Paper II.

4.2. PHOTOCATALYTIC ACTIVITY OF TIO$_2$-GO MATERIALS

Phenol and phenolic compounds are considered by the international organizations as priority contaminants of aquatic systems, since they are harmful for human, animal and plants, even at very low concentration [2,3]. Hence, this research focus on the abatement of 10 ppm phenol in waster solution, as a model polluted water system, under simulated solar light. Samples were taken from the solution every 30 minutes over 3 hours. The details for the photocatalytic set-up system and the testing

procedures are written in Paper II. The schematic of photocatalytic system set-up and the double wall testing reactor are shown in Figure 4-3a and 4-3b, respectively.
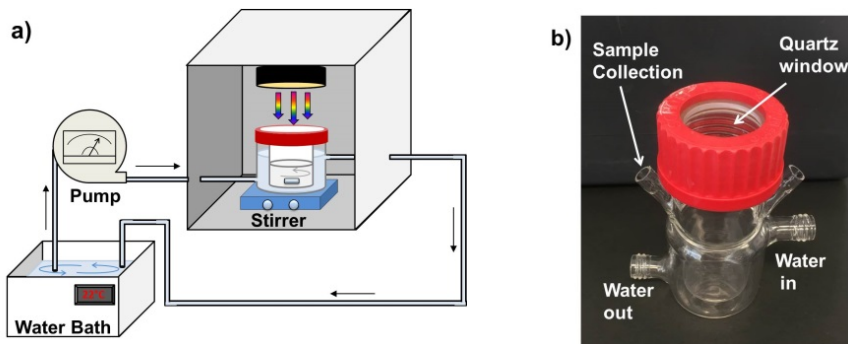
Figure 4-3 a) The schematic of the photocatalytic system set-up and b) double wall photocatalytic reactor are taken from Paper II.

The photodegradation of phenol can be studied via the plot of the normalized concentration ($\frac{C}{C_0}$) as a function the reaction time (t); where C_0 is the starting concentration and C is the concentration at a specific reaction time. The kinetic rate (k) of photocatalytic reaction is determined from the relationship of concentration and reaction time by following the pseudo-first order kinetic, according to equation 4-2. Thus, kinetic constant, k, is obtained from linear regression of the data points in the plot of $-ln\frac{C}{C_0}$ vs. time [120,121].

$$-ln(\frac{C}{C_o}) = kt \qquad\qquad 4-2$$

4.2.1. EFFECT OF GO: TIO$_2$ RATIO

TiO$_2$-GO nanocomposites have been reported to be superior photocatalytic materials, since the formation of an interface between TiO$_2$ and GO can narrow the ban gap energy of TiO$_2$ and can facilitate the electron transfer from TiO$_2$ to GO, thus lowering the electron-hole pairs recombination rate [9,16,24]. However, the GO loading should be consider, since an excess of GO might act as light absorber and prevent the TiO$_2$ photocatalyst materials from the light excitation [16,26,27].

In this section, the photocatalytic activities of the reference TiO$_2$ (TS-100) sample and of GTS-100 composites with various GO loading (0.05, 0.1, 0.2, … and 1 wt%) (synthesized temperature 100°C) are studied. In addition, the different reactors for

synthesis (dynamic condition in the stirring beaker and the static condition in a Teflon vessel) are compared to assess the reproducibility of the material synthesis.

The abatement of 10 ppm phenol under the artificial sunlight is studied via the plot of the normalized concentration ($\frac{c}{c_0}$) as a function of the time, shown in Figure 4-4a. None of the materials show significant degradation of phenol without light (control condition), while the concentration of phenol decreases with time when the artificial sunlight is presented. The reference TiO_2 sample can remove 40% phenol within 180 min. The 0.05GTS-100 and 0.05GTD-100 show 50% of phenol abatement; on the other hand GT composites with 1 wt% GO loading reduce the phenol concentration only of 25% during the same irradiation time.

The reaction rate constant, k, of TiO_2 and GT-GT-100 composites is plotted as a function of the GO loading in Figure 4-4b. The reaction rate of TiO_2 (TS-100) is around $2.8\pm0.1\ 10^{-3}min^{-1}$ that is lower than those of GT-100 composites with GO loading ≤ 0.2 wt%. The maximum k is $3.9\pm0.1\ 10^{-3}min^{-1}$, which was measured for the sample with 0.05 wt% GO loading (0.05GTS-100). This k value is similar to those previously reported in literature for phenol abatement with enhanced GT composites under solar lamp [99,116]. Surprisingly, the GT-100 composites prepared with the stirring Pyrex reactor (0.05GTD-100 and 1GTD-100) have similar k constants to those of the GTS-100 composites, prepared in a static tank.

Figure 4-4 a) The phenol abatement under the controlled condition (dark) and under sun simulator of reference TiO_2 (TS-100) GTS-100 and GTD-100, and b) the rate of photocatalytic reaction of different $GO:TiO_2$ ratio. The Figures are taken from Paper II.

The photodegradation rate constant increases with decreasing GO loading, because the composites have the same morphology, chemical stature, and above all similar interface (see in chapter 3), but show different light adsorption, as discusses in section 4.1. After GO was loaded to TiO_2 at ≥ 0.5 wt%, the rate constants decrease and becomes smaller than that of the pure TiO_2. Furthermore, the from literature we know that the excessive GO prevents TiO_2 photocatalytic centers from light

excitation [16,26]. In addition, the increase of k with decreasing the amount of GO is agree with the results reported by Minella, M. *et al*.[120] and Adamu, H. *et al*.[92].

4.2.2. EFFECT OF SYNTHESIS TEMPERATURE

In section 4.1.2, it was shown how it was possible to obtain photocatalysts with enhanced activity by loading 0.05 wt% GO in TiO_2. Then, this section deals with GT composites with 0.05 wt% GO synthetized with the hydrothermal method in the temperature range 100-200°C, with the aim to study the effect of temperature on the photocatalytic performances of the composites. Samples with 1 wt% GO also studied to investigate the impact of GO loading on the synthesis temperature effects.

Pure TiO_2 synthetized at 200°C (TS-200) can remove 60% of phenol in 180 minutes of irradiation. This is the highest value in Figure 4-5a, i.e. TS-200 has higher k than GTS composites. Among of the GT composites, 0.05GT-200 has the best phenol degradation kinetics ($\sim$ 55%), while all the others GT composites show lower phenol abatement in 3 hours: 45% for 0.05GT-100, 40% for 0.05GT-175 and 1GT-200, and 25% for 1GT-175 and 1GT-200, approximately.

The phenol abatement rate constants are plotted against the synthesis temperature in Figure 4-5b. The figure shows that the maximum photocatalytic rate is $\sim$5.1$\pm$0.1 10^{-3}min^{-1} for TS-200 and k of pure TiO_2 decreases with decreasing synthesis temperature. This can be explained by the observation that the anatase fraction increases with the synthesis temperature and reaches 92% at 200°C.

The dependence of k on the synthesis temperature is more complex for the GT composites than for the pure titania samples and it is influenced by the GO loading. Concerning the 0.05 GTS composites, they were expected to have the highest photocataytic reaction rate over pure TiO_2 and 1GTS composites for each synthesis temperature, like at 100°Cbut the results do not confirm this hypothesis. 0.05GTS-200 has the highest k (4.6$\pm$0.10^{-3}min^{-1}), while the 0.05 GTS-175 nanocomposite has the lowest (2.9$\pm$0.1 10^{-3}min^{-1}). These results can be explained by considering the microstructure of these samples. The HRTEM pictures in Figure 3-10a -3-10c show that the sample prepared at 175°C consists of TiO_2 nanoparticles surrounded by thick amorphous carbon, which can shield the TiO_2 photocatalytic center from the light resulting in a decline of k. Hence, its photodegradation rate is lower than that of pure TS-200. Furthermore, previous studies suggest that the best photocatalytic ability of GT composites is obtained when TiO_2 nanoparticles interact with GO monolayers (rather than GO nanoribbons) since, under these conditions, the charge transfer from TiO_2 to GO is the most effective [122] and competitive light abortion from GO is limited.

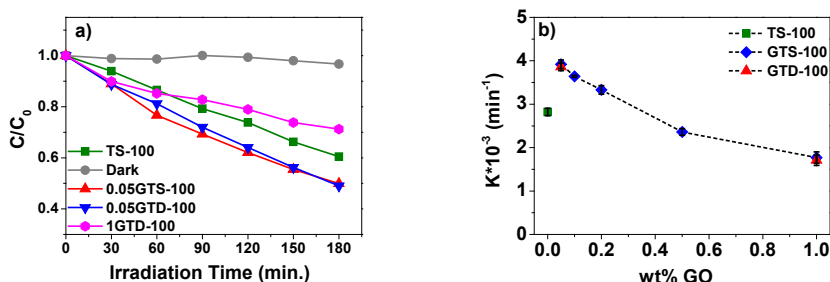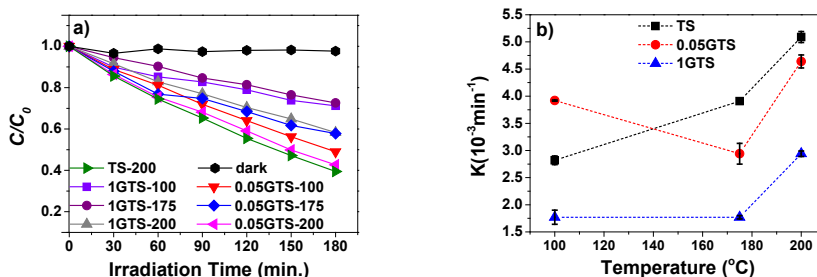*Figure 4-5 a) The phenol abatement under the controlled condition (dark) and under sun simulator of reference TiO$_2$ (TS-200), 0.05GTS and 1GTD synthesis from 100-200°C and b) the rate of photocatalytic reaction of different temperature of hydrothermal synthesis.*

4.3. SUMMARY

In this chapter, GT nanocomposites, synthetized under mild conditions via simple sol-gel method, have been proven to be effective in the abatement of phenol under simulated solar light. The impact of GO loading and synthesis temperature on the phenol degradation rate constant was discussed. Light absorption in UV-Vis range of GT composite increases with increasing the amount of GO doping, however this has little impact on the band gap energy of the GT nanocomposites. For samples synthetized at 100 °C, the phenol photodegradation rate constant increases with decreasing the GO loading, and reaches the maximum value (3.9 ± 0.1 10^{-3}min^{-1}) for the sample prepared with 0.05 wt% of GO. However, the sample prepared with the hydrothermal method at 200°C with the same amount of GO has a higher photocatalytic reaction rate constant: 4.6 ± 0.1 10^{-3}min^{-1}. This might be due to a different interface bonding (both Ti-O-C and Ti-C are present in 0.05GTS-200) and higher degree of reduction of GO. Nevertheless, the dependence of the photocatalytic performances of the GT nanocomposites on their synthesis temperature is rather complex, because under certain conditions, core-shell TiO$_2$-graphitic or amorphous carbon are formed, hindering light exploitation. According to our results, such type of structures is stabilized during hydrothermal synthesis at 175°C, and hence this temperature should be avoided for the synthesis of GT composites.

CHAPTER 5. TIO$_2$-GO PHOTOCATALYTIC MEMBRANES

One important application of TiO$_2$-GO is the fabrication of membranes for water filtration application, since this type of materials in principle can offer high water permeability, while separating and degrading organic pollutants and preventing membrane fouling. In addition, the incorporation of TiO$_2$-GO nanopowder into GO based membrane is considered as immobilization method for recovery of the photocatalytic powder from the water after purification [32].

GO and TiO$_2$-GO membranes were prepared via a simple vacuum filtration method, that is, by filtering a dispersion of GO and TiO$_2$ nanoparticles through a commercial polymer filter. In this way, membrane thickness can be easily tuned by varying the concentration or the volume of the dispersion. SEM and XRD analysis was performed to investigate the morphology of the membranes and to check the presence of defects.

5.1. PREPARATION OF TIO$_2$-GO BASED MEMBRANES

In this study, the commercial TiO$_2$ nanopowerder P25 was used as photocatalytis for studying the method of preparation of GO-TiO$_2$ membranes. After optimizing the fabrication procedure, 0.05GTS-200 and other of the photocatalytic materials reported in Chapter 3 and 4 will be eventually applied to prepare GO-TiO$_2$ membranes.

The preparation method adopted in this work is based on the study of Zhu, C. *et al.* [93]. The schematic of GO based membrane preparation is shown in Figure 5-1. GO was dispersed in ultrapure water (0.01 wt%) by sonication for 3 hours, thus obtaining the GO suspension hereinafter named "suspension A". P25 (Average particle size ~ 21 nm) was dispersed in ultrapure water (0.01 wt%) by sonication for 1 hour, thus obtaining the TiO$_2$ suspension hereinafter named "suspension B".

Pure GO membranes were prepared by taking different volumes of "suspension A", e.g. 2.5, 5.0, 7.5,… and 20 ml to obtain 0.25, 0.5, 0.75, … and 2 mg of GO and mixed with ultrapure water to a total volumes for 50 ml. The so obtained dispersion were sonicated for 30 min and then filtered over a mixed cellulose ester (MCE) filter (pore size = 0.22 μm, diameter = 47 mm). After removing water, the GO membrane was maintained for 30 minutes under the vacuum to obtain a compact structure. The membrane was dried at the room temperature overnight.

The TiO_2-GO membranes were made by a similar method to GO membranes. Selected volumes of suspension A and B were taken and mixed in a beaker together with water to reach a volume of 50 mL, and sonicated for 2 hours. The final dispersions contained 1.0 mg of GO and the weight ratio between TiO_2 and GO 0.5, 1, 2 and 4.
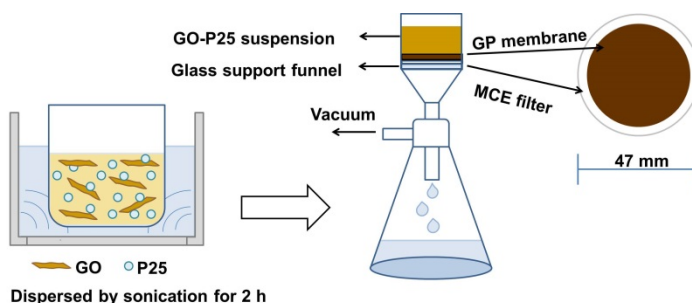
Figure 5-1 Schematic of GO based membrane preparation.

5.2. MEMBRANE MORPHOLOGY

5.2.1. MORPHOLOGY OF GO MEMBRANES

The GO membrane named 0.25GO, 0.5GO, 0.75GO, 1GO and 2GO were prepared from 50 ml dispersions containing 0.25, 0.5, 0.75, 1 and 2 mg of GO, respectively. These membranes are shown in in Figure 5-2a. The higher was the concentration of GO in the dispersion, the darker is the color of the membrane. Homogenous GO membranes were obtained GO loading down to 0.5 mg of. On the contrary, the 0.25GO sample consists of a non-continuous, as indicated by the red circle in the figure. The structure and the thickness of these membranes were investigated by SEM analysis. The micrographs (Figures 5-2b – 5-2e) show the highly polymer substrate and the typical layered structure of thin GO membranes, which also present winkled surface The estimated thickness of the GO films is plotted in the Figures 5-3 as a function of the GO loading in filtered dispersion. It ranges from 0.2 to 1.39 μm from 0.5 GO to 2GO.
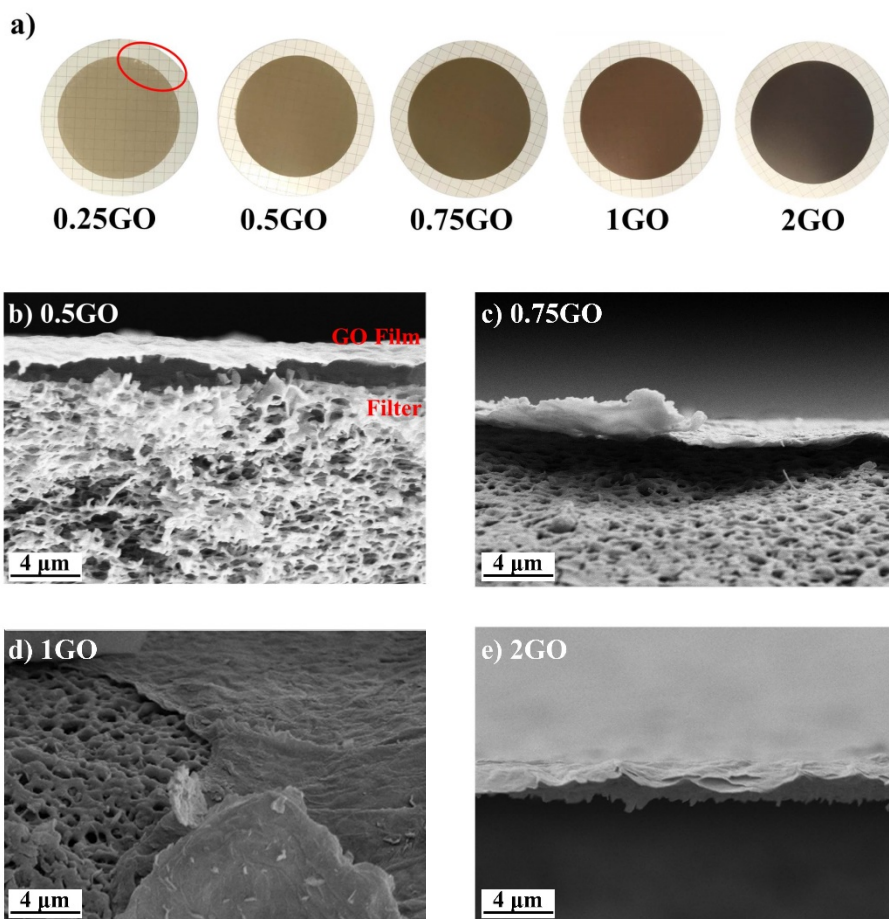
Figure 5-2 a) Digital photographs and b) SEM pictures of GO membranes
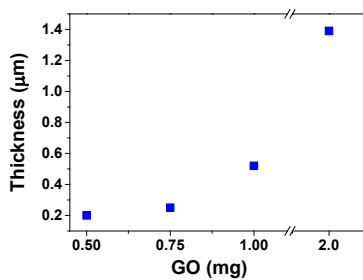
Figure 5-3 Thickness of GO membranes as a function of the GO mass in the dispersion used for membrane fabrication (filter diameter = 47 mm).

5.2.2. MORPHOLOGY OF TIO$_2$-GO MEMBRANES

TiO$_2$-GO membranes by doping P25 in different amount; 0.5, 1, 1, 2 and 4 mg, resulting 1:0.5GT, 1:1GT, 1:2GT and 1:4GT, respectively. The ratio of GO to TiO$_2$ for making the membrane is based on previous papers, which reported the results about the selectivity and photocatalytic performances of membranes prepared with similar methods [93,96].

After adding TiO$_2$ nanoparticles to GO, the composite films present rougher surface and their thickness increases up to maximum of about 1.2 μm, as it can be observed in Figure 5-4. In addition, the samples with low TiO$_2$, namely 1:0.5GT, 1:1GT, present the typical lamellar structure of GO membranes, while 1:2GT and 1:4GT present a different type of structure, which is characterized by aggregates of TiO$_2$ nanoparticles.
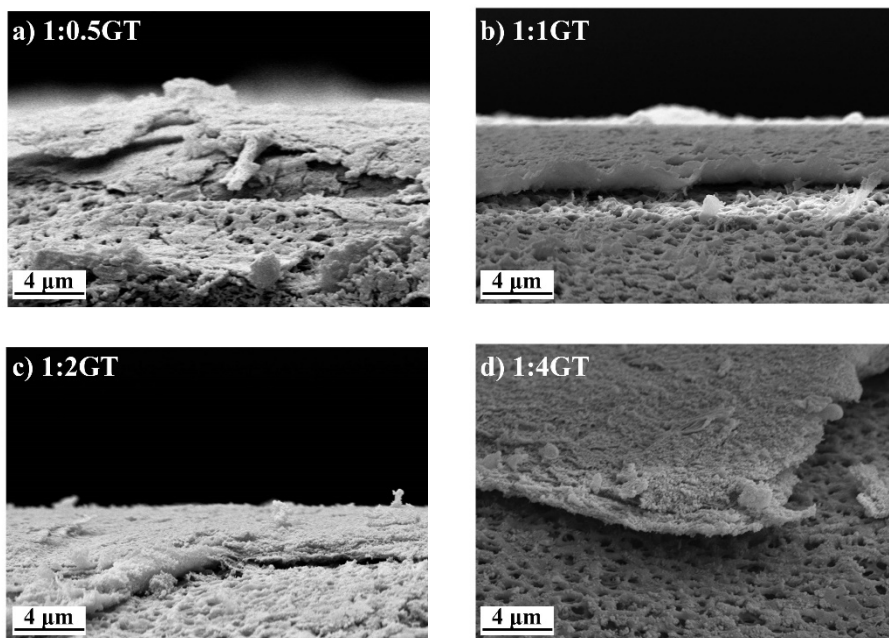
Figure 5-4 SEM pictures of GT membranes.

The XRD patterns of the TiO$_2$-GO (GT) membranes are shown in Figure 5-5a. The diffractogram of the MCE filter is reported as reference. It has two broad peaks with center at *2θ* =11.4° and 21.2°. This curve was used for baseline subtraction in the analysis of the other diffractograms. In the XRD patterns of all the membranes it is possible to observe the characteristic peak of the fully oxidized graphene oxide at *2θ* of about 10.8° for GO and at 10.5°-10.6° for GT. The peak position and FWHT were

used to calculate the interlayer (*d*)-space and the average thickness of graphene oxide domains, respectively. The interlayer distance of the GO membrane is estimated ~8.2 Å, while that of the GT membranes is 8.3-8.5 Å. Therefore TiO_2 intercalation has little effect on the *d*-space. In the case of the GT membranes, the position of this peak does not change with increasing the TiO_2 loading, but the peak becomes less intense and broader. The Scherrer thickness of graphene oxide domains in the pure GO membranes is 14.4 nm. Figure 5-5b shows that this distance decreases with increasing the TiO_2 loading, meaning that TiO_2 nanoparticles can be incorporated into GO layers by reducing the thickness of GO nanoribbons (Figure 5-5b). The intensity of the TiO_2 characteristic peaks becomes stronger with increasing the TiO_2 loading. Only the anatase peak at 2θ =25.5° is visible in 1:0.5GT, while the rutile peak at $\sim2\theta$ =27.5 can be clearly seen from 2 mg of TiO_2 loading.
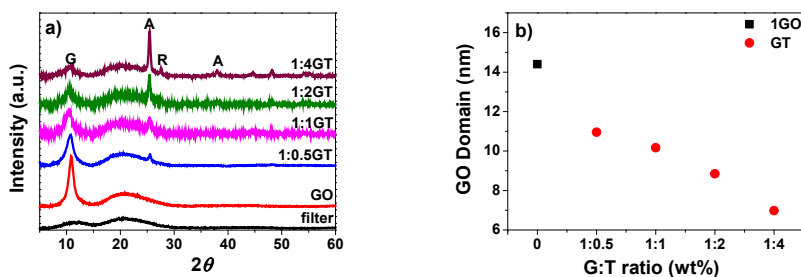
Figure 5-5 a) XRD patterns of the bare filter and of the supported GO and GT membranes and b) the GO domain of GO and GT membranes. G, A, and R stand for the characteristic peaks of GO, anatase TiO_2 and rutile TiO_2 phases, respectively.

5.3. MEMBRANE TESTING

Over the recent years, a few papers dealt with the use of TiO_2-GO membranes for water depollution. However, most of the tests were done under unrealistic conditions: e.g. in the dead-end systems, with dye solutions as model water systems, and under UV irradiation [93]. Therefore, this study focuses on the testing of TiO_2-GO membranes for the abatement of organic pollutants in real wastewater systems. For this reason, the cross-flow filtration system has been designed, which is depicted in Figure 5-6a, and the cross-flow testing reactor is displayed in Figure 5-6b. This membrane photo-reactor consists of a stainless steel housing with a 35 mm quartz window for exploiting sunlight or simulated solar light during filtration (more details of the sun simulator are given in Paper II). At the time when this thesis was submitted, the membrane photo-reactor had been tested only with the pure GO membrane, namely with the 1GO sample. The GO film started to exfoliate after 3 hours of testing time, meaning that the GO membrane is not stable under this condition. This type of instability was already observed for pure GO membranes prepared via pressure-assisted self-assembly [60]. Chemical crosslink, e.g. with

ethylenediamine [123], have been proposed for stabilizing GO membranes. It is not clear at this stage if TiO_2 nanoparticles, which are anchored on GO sheets by Ti-O-C bond can act as cross-linkers, thus stabilizing the GO membrane structure during filtration. Otherwise, TiO_2-GO membranes would be required further stabilization by molecular cross-linkers. Once these stability problems are solved, TiO_2-GO membranes should be tested with phenol solutions, as model systems, to assess the ability to concentrate and degrade organic pollutants. Moreover, water solutions of humic acids, which are typical fouling agents [124], will be used for study the self-cleaning properties of the new membranes.
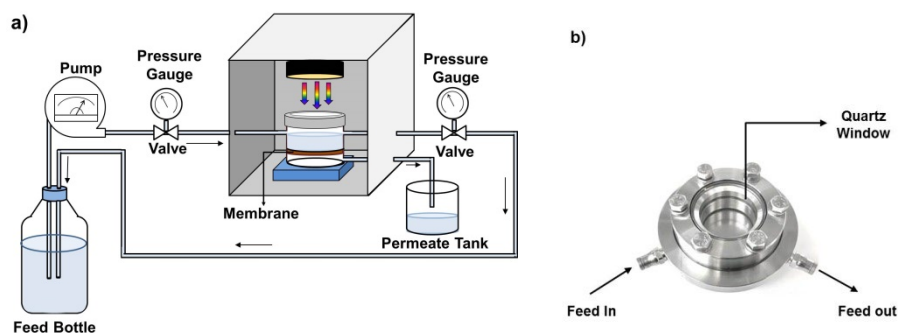
Figure 5-6 a) The schematic of cross-flow testing system and b) the crossflow testing reactor

5.4. SUMMARY

Graphene based membranes were prepared by vacuum filtration. Membrane thickness was varied from 0.2 to 1.4 μm by adjusting the concentration of the filtered GO suspension. The introduction of TiO_2 nanoparticles has little influence on the space between GO layers, which is 8.3-8.5 Å for all the membranes. However, TiO_2 nanoparticles can decrease the thickness of GO ribbons from 14 nm to less than 11 nm, depend on the TiO_2 loading. A photocatalytic cross-flow membrane reactor was designed and assembled for testing the photocatalytic performances of the new membranes in the abatement of organic pollutants and their self-cleaning properties.

CHAPTER 6.
CONCLUSIONS AND PERSPECTIVES

6.1. CONCLUSIONS

Although TiO_2-GO photocatalytic materials have been investigated over last two decades, the study of the interface bonding between TiO_2 and GO is still challenging. It is crucial to understand the influence of this bonding on the physical and chemical behaviors of the TiO_2-GO composite materials used for the photocatalytic degradationThis subject is still largely unexplored. In this Ph.D. thesis, various factors were studied, which relate the structure of TiO_2-GO nanocomposites to their final photocatalytic properties.

In this work, great attention was given to the interface bonding, which is an important feature that determines physical and chemical properties of TiO_2-GO materials. We succeeded in the conjugation of TiO_2 and GO with Ti-O-C bonding by synthetizing the TiO_2-GO composites in mild conditions: pH = 6 and temperature of 100°C. This interface interaction has a strong influence also on the transition temperatures of both materials: from graphene oxide to reduced graphene oxide at and from amorphous TiO_2 to anatase. Furthermore, we obtained Ti-C bonding after hydrothermal treatment at T ≥ 175°C for 4 hours. Our results are similar to those studied previously where Ti-C bonding was formed upon annealing at 400°C [113], hydrothermal treatment at 200°C for 10 hours [90], or by in-situ nucleation and growth at 110°C for 24 hours and followed by curing at 145°C for 72 hours [114]. Therefore, our methods are easy to prepare TiO_2-GO composites with interface bonding.

The photocatalytic activity of TiO_2-GO composites depends on many factors such as the morphology, the interface bonding, the band gap energy, the condition of photocatalytic testing, and organic pollutants to be degraded. In this study, the phenol abatement under solar simulation was studied depending of different synthesis parameters:

i) The amount of GO loading, as the varied amount of GO loading shows significant difference of photocatalytic degradation rate. Loading of GO over 0.2 wt% results in a lower photocatalytic activity than pure TiO_2, while lower amount than 0.2 wt% GO allows for higher photodegradation rates. This was explained by the possible scenario that the excess of GO shields the TiO_2 photocatalytic center from light exploitation.

ii)   The phase fraction of anatase, as the photocatalytic activity increases with increase of the amount of anatase. This can be confirmed by the photocatalytic activity of pure titania photocatalyst prepared at 200°C which is higher than the catalysts synthetized at a lower temperature. GTS-100 has ~80% of anantase and GT-200°C has ~92% of anantase.

iii) The interface bonding could encourage the photocatalytic activity by promoting the electron transfer from TiO_2 to GO. In this study, we found 2 types of bonding namely Ti-C-O and Ti-C that arise in different temperatures; respectively at 100°C and $\geq$ 175°C. However, the GT composites prepared at 175-200°C do not exhibit excellent photocatalytic activity, even though they have both types of interface bonding with prevalence of bonding created at 175°C. It could be hypothesized that, at this temperature, TiO_2-rGO from core-shell structures with shell thickness around 3.8-5 nm (0.05GTS-175), which shield TiO_2 nanoparticles from light and might prevent radical formation before recombination of electron-hole pairs [122,125]. It was suggested that better photocatalytic activity is obtained from TiO_2 nanoparticles deposited on monolayer (one atomic thickness, ~ 0.34 nm, theoretical).

iv)   The degree of reduction of GO, as reducing oxygen functional groups promotes the electron transfer from the TiO_2 photocatalytic center to rGO, due to higher electron conductivity of rGO than GO [116]. The results of XPS analysis based on calculation of the partial reduction of GO (A_{C-O}/A_{C-C} and $A_{O=C=O}/A_{C-C}$) show that 1GTS-200 has higher reduction than 1GTS-100. Samples prepared with 0.05 wt% GO loading shall have a similar reduction degree. However, the photocatalytic activity of 0.05GT composites prepared at higher temperature is lower than expected. It could be due to the morphology of GT composites that is explained above.

The optimal structure for these photocatalysts consist in TiO_2 nanoparticles laying on isolated GO, sheets, as we can assume that one layer of GO is transparent. We observed this structure only during synthesis at 100°C with addition of 0.05 wt% GO. Higher amount of GO and higher synthesis temperature cause the formation of GO nanoribbons and/or core-shell structure of TiO_2 nanoparticles surrounded by amorphous carbon or restacked rGO. These types of structure do not allow for efficient exploitation of the solar light. Remarkably in this study, no significantly different values of the band gap energy were obtained for our materials, and therefore their photocatalytic performances are strongly related to their morphology.

In the preparation of TiO_2-GO base membranes, the fabrication method and the intercalation with TiO_2 nanoparticles are important for the filtration ability. GO membranes prepared without any crossly-linker are not stable for longer time under cross-flow conditions and therefore they are not suitable for water filtration. In

addition, the intercalation with TiO_2 nanoparticles cannot change the interspace between GO planes. It can only decrease the thickness of restacking GO, which might prevent the improvement of the water permeation rate. At this stage, it is not clear that TiO_2 nanoparticles, in reason of the Ti-O-C bonding, can actually act as cross-linkers thus stabilizing GO-TiO_2 during filtration.

6.2. PERSPECTIVES

This project resulted in obtaining promising TiO_2-GO photocatalytic materials for application in the water purification technologies. The preparation of such materials was performed via an environmental friendly method, which involved low energy consumption methods and mild reaction conditions. Nevertheless, the most important outcome of this study is the development of new understanding on how the synthesis conditions influence the structure of TiO_2-GO nanocomposite and thus their photodegradation performances. This new knowledge can support the rational design of TiO_2-GO materials with enhanced photocatalytic properties. The outcomes of this thesis suggest further studies on the following two research problems.

Higher photodegradation rates might be obtained by avoiding the formation of carbon/rGO-shell structures which cause lowering of photodegradation rate. The suggestion is to synthesis 0.05GT with hydrothermal route at temperature above 200°C. In this way it can be possible to obtain 100% anatase. This should help to avoid the TiO_2 nanoparticles encapsulation as by synthesis at above 200°C less carbon shell structures are created, due to the braking of the rGO basal plane. The photocatalytic tests using solar light have to be conducted with other organic substrates and with real wastewater samples to assess the ability of this photocatalyst to work under realistic conditions. Moreover, the ability of the photocatalysts to inactivate pathogens might be checked.

GO-TiO_2 membranes have to be prepared by using cross-linkers to improve their mechanical stability. In addition, the concentration of GO should be lowered as thick films have low water permeability and are opaque. Another option is to use other techniques for membrane fabrication, e.g., casting blade to obtain thinner films, which will be more transparent, and thus will allow light to reach TiO_2 particles. In addition, by using layer by layer techniques, it could be possible to obtain higher photocatalytic activity by coating GO film with TiO_2 nanoparticles. In this way it will be possible to concentrate organic molecules on top of the membrane, while photodegradation occurs on the membrane surface because of the TiO_2 photocatalytic centers.

BIBLIOGRAPHY

[1]   B. Petrie, R. Barden, B. Kasprzyk-Hordern, A review on emerging contaminants in wastewaters and the environment: Current knowledge, understudied areas and recommendations for future monitoring, Water Research. 72 (2015) 3–27. doi:10.1016/j.watres.2014.08.053.

[2]   L.G.C. Villegas, N. Mashhadi, M. Chen, D. Mukherjee, K.E. Taylor, N. Biswas, A Short Review of Techniques for Phenol Removal from Wastewater, Curr Pollution Rep. 2 (2016) 157–167. doi:10.1007/s40726-016-0035-3.

[3]   W.W. Anku, M.A. Mamo, P.P. Govender, Phenolic Compounds in Water: Sources, Reactivity, Toxicity and Treatment Methods, (2017). doi:10.5772/66927.

[4]   T. Deblonde, C. Cossu-Leguille, P. Hartemann, Emerging pollutants in wastewater: A review of the literature, International Journal of Hygiene and Environmental Health. 214 (2011) 442–448. doi:10.1016/j.ijheh.2011.08.002.

[5]   M. Elma, C. Yacou, D.K. Wang, S. Smart, J.C. Diniz da Costa, Microporous Silica Based Membranes for Desalination, Water. 4 (2012) 629–649. doi:10.3390/w4030629.

[6]   The United Nations world water development report, 2017: Wastewater: the untapped resource - UNESCO Digital Library, (n.d.).   https://unesdoc.unesco.org/ark:/48223/pf0000247153 (accessed January 15, 2019).

[7]   E. Rafiee, E. Noori, A.A. Zinatizadeh, H. Zanganeh, Photocatalytic degradation of phenol using a new developed TiO2/graphene/heteropoly acid nanocomposite: synthesis, characterization and process optimization, RSC Adv. 6 (2016) 96554–96562. doi:10.1039/C6RA09897E.

[8]   M. Faraldos, A. Bahamonde, Environmental applications of titania-graphene photocatalysts, Catalysis Today. 285 (2017) 13–28. doi:10.1016/j.cattod.2017.01.029.

[9]   Y. Jiang, W.-N. Wang, D. Liu, Y. Nie, W. Li, J. Wu, F. Zhang, P. Biswas, J.D. Fortner, Engineered crumpled graphene oxide nanocomposite membrane assemblies for advanced water treatment processes, Environ. Sci. Technol. 49 (2015) 6846–6854. doi:10.1021/acs.est.5b00904.

[10] O. Ola, M.M. Maroto-Valer, Review of material design and reactor engineering on TiO$_2$ photocatalysis for CO$_2$ reduction, Journal of Photochemistry and Photobiology C: Photochemistry Reviews. 24 (2015) 16–42. doi:10.1016/j.jphotochemrev.2015.06.001.

[11] M. Pelaez, N.T. Nolan, S.C. Pillai, M.K. Seery, P. Falaras, A.G. Kontos, P.S.M. Dunlop, J.W.J. Hamilton, J.A. Byrne, K. O'Shea, M.H. Entezari, D.D. Dionysiou, A review on the visible light active titanium dioxide photocatalysts for environmental applications, Applied Catalysis B: Environmental. 125 (2012) 331–349. doi:10.1016/j.apcatb.2012.05.036.

[12] L.-L. Tan, S.-P. Chai, A.R. Mohamed, Synthesis and Applications of Graphene-Based TiO$_2$ Photocatalysts, ChemSusChem. 5 (2012) 1868–1882. doi:10.1002/cssc.201200480.

[13] R.K. Upadhyay, N. Soin, S.S. Roy, Role of graphene/metal oxide composites as photocatalysts, adsorbents and disinfectants in water treatment: a review, RSC Adv. 4 (2013) 3823–3851. doi:10.1039/C3RA45013A.

[14] P. Calza, C. Hadjicostas, V.A. Sakkas, M. Sarro, C. Minero, C. Medana, T.A. Albanis, Photocatalytic transformation of the antipsychotic drug risperidone in aqueous media on reduced graphene oxide—TiO$_2$ composites, Applied Catalysis B: Environmental. 183 (2016) 96–106. doi:10.1016/j.apcatb.2015.10.010.

[15] R. Giovannetti, E. Rommozzi, M. Zannotti, C.A. D'Amato, Recent Advances in Graphene Based TiO2 Nanocomposites (GTiO2Ns) for Photocatalytic Degradation of Synthetic Dyes, Catalysts. 7 (2017) 305. doi:10.3390/catal7100305.

[16] M. Nawaz, W. Miran, J. Jang, D.S. Lee, One-step hydrothermal synthesis of porous 3D reduced graphene oxide/TiO$_2$ aerogel for carbamazepine photodegradation in aqueous solution, Applied Catalysis B: Environmental. 203 (2017) 85–95. doi:10.1016/j.apcatb.2016.10.007.

[17] N. Zhang, M.-Q. Yang, S. Liu, Y. Sun, Y.-J. Xu, Waltzing with the Versatile Platform of Graphene to Synthesize Composite Photocatalysts, Chem. Rev. 115 (2015) 10307–10377. doi:10.1021/acs.chemrev.5b00267.

[18]   F. Perreault, A.F. de Faria, M. Elimelech, Environmental applications of graphene-based nanomaterials, Chem. Soc. Rev. 44 (2015) 5861–5896. doi:10.1039/C5CS00021A.

[19]   R. Sadri, K.Z. Kamali, M. Hosseini, N. Zubir, S.N. Kazi, G. Ahmadi, M. Dahari, N.M. Huang, A.M. Golsheikh, Experimental study on thermo-physical and rheological properties of stable and green reduced graphene oxide nanofluids: Hydrothermal assisted technique, Journal of Dispersion Science and Technology. 38 (2017) 1302–1310. doi:10.1080/01932691.2016.1234387.

[20]   C. Hu, T. Lu, F. Chen, R. Zhang, A brief review of graphene–metal oxide composites synthesis and applications in photocatalysis, Journal of the Chinese Advanced Materials Society. 1 (2013) 21–39. doi:10.1080/22243682.2013.771917.

[21]   V. Boffa, D.G. Perrone, G. Magnacca, E. Montoneri, Role of a waste-derived polymeric biosurfactant in the sol–gel synthesis of nanocrystalline titanium dioxide, Ceramics International. 40 (2014) 12161–12169. doi:10.1016/j.ceramint.2014.04.056.

[22]   K. Gigant, A. Rammal, M. Henry, Synthesis and Molecular Structures of Some New Titanium(IV) Aryloxides, J. Am. Chem. Soc. 123 (2001) 11632–11637. doi:10.1021/ja016930f.

[23]   T.N. Lambert, C.A. Chavez, B. Hernandez-Sanchez, P. Lu, N.S. Bell, A. Ambrosini, T. Friedman, T.J. Boyle, D.R. Wheeler, D.L. Huber, Synthesis and Characterization of Titania−Graphene Nanocomposites, J. Phys. Chem. C. 113 (2009) 19812–19823. doi:10.1021/jp905456f.

[24]   J. Jing, Y. Zhang, W. Li, W.W. Yu, Visible light driven photodegradation of quinoline over TiO_2/graphene oxide nanocomposites, Journal of Catalysis. 316 (2014) 174–181. doi:10.1016/j.jcat.2014.05.009.

[25]   Y. Min, K. Zhang, W. Zhao, F. Zheng, Y. Chen, Y. Zhang, Enhanced chemical interaction between TiO_2 and graphene oxide for photocatalytic decolorization of methylene blue, Chemical Engineering Journal. 193–194 (2012) 203–210. doi:10.1016/j.cej.2012.04.047.

[26]   D. Pan, J. Jiao, Z. Li, Y. Guo, C. Feng, Y. Liu, L. Wang, M. Wu, Efficient Separation of Electron–Hole Pairs in Graphene Quantum Dots by TiO_2 Heterojunctions for Dye Degradation,

ACS Sustainable Chem. Eng. 3 (2015) 2405–2413. doi:10.1021/acssuschemeng.5b00771.

[27] P. Wang, J. Wang, X. Wang, H. Yu, J. Yu, M. Lei, Y. Wang, One-step synthesis of easy-recycling TiO_2-rGO nanocomposite photocatalysts with enhanced photocatalytic activity, Applied Catalysis B: Environmental. 132–133 (2013) 452–459. doi:10.1016/j.apcatb.2012.12.009.

[28] S.M. El-Sheikh, T.M. Khedr, A. Hakki, A.A. Ismail, W.A. Badawy, D.W. Bahnemann, Visible light activated carbon and nitrogen co-doped mesoporous TiO_2 as efficient photocatalyst for degradation of ibuprofen, Separation and Purification Technology. 173 (2017) 258–268. doi:10.1016/j.seppur.2016.09.034.

[29] J. Choina, H. Kosslick, C. Fischer, G.-U. Flechsig, L. Frunza, A. Schulz, Photocatalytic decomposition of pharmaceutical ibuprofen pollutions in water over titania catalyst, Applied Catalysis B: Environmental. 129 (2013) 589–598. doi:10.1016/j.apcatb.2012.09.053.

[30] T. Wang, Z. Xu, L. Wu, B. Li, M. Chen, S. Xue, Y. Zhu, J. Cai, Enhanced photocatalytic activity for degrading phenol in seawater by TiO2-based catalysts under weak light irradiation, RSC Adv. 7 (2017) 31921–31929. doi:10.1039/C7RA04732K.

[31] A.K. Nair, J. P.e., TiO_2 nanosheet-graphene oxide based photocatalytic hierarchical membrane for water purification, Surface and Coatings Technology. 320 (2017) 259–262. doi:10.1016/j.surfcoat.2017.01.022.

[32] Y. Gao, M. Hu, B. Mi, Membrane surface modification with TiO2–graphene oxide for enhanced photocatalytic performance, Journal of Membrane Science. 455 (2014) 349–356. doi:10.1016/j.memsci.2014.01.011.

[33] O.C. Compton, S.T. Nguyen, Graphene Oxide, Highly Reduced Graphene Oxide, and Graphene: Versatile Building Blocks for Carbon-Based Materials, Small. 6 (2010) 711–723. doi:10.1002/smll.200901934.

[34] D. Chen, H. Feng, J. Li, Graphene Oxide: Preparation, Functionalization, and Electrochemical Applications, (2012). doi:10.1021/cr300115g.

[35] A.K. Geim, K.S. Novoselov, The rise of graphene, Nature Materials. 6 (2007) 183–191. doi:10.1038/nmat1849.

[36]   G. Zhao, X. Li, M. Huang, Z. Zhen, Y. Zhong, Q. Chen, X. Zhao, Y. He, R. Hu, T. Yang, R. Zhang, C. Li, J. Kong, J.-B. Xu, R.S. Ruoff, H. Zhu, The physics and chemistry of graphene-on-surfaces, Chem. Soc. Rev. 46 (2017) 4417–4449. doi:10.1039/C7CS00256D.

[37]   V. Chabot, D. Higgins, A. Yu, X. Xiao, Z. Chen, J. Zhang, A review of graphene and graphene oxide sponge: material synthesis and applications to energy and the environment, Energy Environ. Sci. 7 (2014) 1564–1596. doi:10.1039/C3EE43385D.

[38]   H.M. Hegab, L. Zou, Graphene oxide-assisted membranes: Fabrication and potential applications in desalination and water purification, Journal of Membrane Science. 484 (2015) 95–106. doi:10.1016/j.memsci.2015.03.011.

[39]   S. Stankovich, D.A. Dikin, R.D. Piner, K.A. Kohlhaas, A. Kleinhammes, Y. Jia, Y. Wu, S.T. Nguyen, R.S. Ruoff, Synthesis of graphene-based nanosheets via chemical reduction of exfoliated graphite oxide, Carbon. 45 (2007) 1558–1565. doi:10.1016/j.carbon.2007.02.034.

[40]   Y. Liu, Hydrothermal synthesis of TiO$_2$–RGO composites and their improved photocatalytic activity in visible light, RSC Adv. 4 (2014) 36040–36045. doi:10.1039/C4RA06342B.

[41]   S.F. Kiew, L.V. Kiew, H.B. Lee, T. Imae, L.Y. Chung, Assessing biocompatibility of graphene oxide-based nanocarriers: A review, Journal of Controlled Release. 226 (2016) 217–228. doi:10.1016/j.jconrel.2016.02.015.

[42]   Abid, P. Sehrawat, S.S. Islam, P. Mishra, S. Ahmad, Reduced graphene oxide (rGO) based wideband optical sensor and the role of Temperature, Defect States and Quantum Efficiency, Scientific Reports. 8 (2018) 3537. doi:10.1038/s41598-018-21686-2.

[43]   C. Cha, S.R. Shin, N. Annabi, M.R. Dokmeci, A. Khademhosseini, Carbon-Based Nanomaterials: Multi-Functional Materials for Biomedical Engineering, ACS Nano. 7 (2013) 2891–2897. doi:10.1021/nn401196a.

[44]   X. Wang, E.N. Kalali, J.-T. Wan, D.-Y. Wang, Carbon-family materials for flame retardant polymeric materials, Progress in Polymer Science. 69 (2017) 22–46. doi:10.1016/j.progpolymsci.2017.02.001.

[45] W.-N. Wang, Y. Jiang, P. Biswas, Evaporation-Induced Crumpling of Graphene Oxide Nanosheets in Aerosolized Droplets: Confinement Force Relationship, J. Phys. Chem. Lett. 3 (2012) 3228–3233. doi:10.1021/jz3015869.

[46] J. Wang, X. Gao, Y. Wang, C. Gao, Novel graphene oxide sponge synthesized by freeze-drying process for the removal of 2,4,6-trichlorophenol, RSC Advances. 4 (2014) 57476–57482. doi:10.1039/C4RA09995H.

[47] X. Zhang, P. Suresh Kumar, V. Aravindan, H.H. Liu, J. Sundaramurthy, S.G. Mhaisalkar, H.M. Duong, S. Ramakrishna, S. Madhavi, Electrospun TiO_2–Graphene Composite Nanofibers as a Highly Durable Insertion Anode for Lithium Ion Batteries, J. Phys. Chem. C. 116 (2012) 14780–14788. doi:10.1021/jp302574g.

[48] B.E. Warren, P. Bodenstein, The shape of two-dimensional carbon black reflections, Acta Cryst, Acta Crystallogr. 20 (1966) 602–605. doi:10.1107/S0365110X66001464.

[49] M. Safarpour, A. Khataee, V. Vatanpour, Preparation of a Novel Polyvinylidene Fluoride (PVDF) Ultrafiltration Membrane Modified with Reduced Graphene Oxide/Titanium Dioxide (TiO_2) Nanocomposite with Enhanced Hydrophilicity and Antifouling Properties, Ind. Eng. Chem. Res. 53 (2014) 13370–13382. doi:10.1021/ie502407g.

[50] Electrospun titania nanofibers segregated by graphene oxide for improved visible light photocatalysis, (n.d.). http://www.sciencedirect.com/science/article/pii/S0926337316306646 (accessed November 23, 2016).

[51] W. Wang, J. Yu, Q. Xiang, B. Cheng, Enhanced photocatalytic activity of hierarchical macro/mesoporous TiO_2–graphene composites for photodegradation of acetone in air, Applied Catalysis B: Environmental. 119–120 (2012) 109–116. doi:10.1016/j.apcatb.2012.02.035.

[52] Y. Shen, S. Yang, P. Zhou, Q. Sun, P. Wang, L. Wan, J. Li, L. Chen, X. Wang, S. Ding, D.W. Zhang, Evolution of the band-gap and optical properties of graphene oxide with controllable reduction level, Carbon. 62 (2013) 157–164. doi:10.1016/j.carbon.2013.06.007.

[53] B. Yu, X. Wang, X. Qian, W. Xing, H. Yang, L. Ma, Y. Lin, S. Jiang, L. Song, Y. Hu, S. Lo, Functionalized graphene

oxide/phosphoramide oligomer hybrids flame retardant prepared via in situ polymerization for improving the fire safety of polypropylene, RSC Adv. 4 (2014) 31782–31794. doi:10.1039/C3RA45945D.

[54] S. Eigler, S. Grimm, F. Hof, A. Hirsch, Graphene oxide: a stable carbon framework for functionalization, Journal of Materials Chemistry A. 1 (2013) 11559–11562. doi:10.1039/C3TA12975F.

[55] W. Zhang, Y. Li, S. Peng, Facile Synthesis of Graphene Sponge from Graphene Oxide for Efficient Dye-Sensitized H2 Evolution, ACS Appl. Mater. Interfaces. 8 (2016) 15187–15195. doi:10.1021/acsami.6b01805.

[56] W.L. Zhang, H.J. Choi, Fast and facile fabrication of a graphene oxide/titania nanocomposite and its electro-responsive characteristics, Chem. Commun. 47 (2011) 12286–12288. doi:10.1039/C1CC14983K.

[57] J.I. Paredes, S. Villar-Rodil, A. Martínez-Alonso, J.M.D. Tascón, Graphene Oxide Dispersions in Organic Solvents, Langmuir. 24 (2008) 10560–10564. doi:10.1021/la801744a.

[58] Z. Ji, G. Zhu, X. Shen, H. Zhou, C. Wu, M. Wang, Reduced graphene oxide supported FePt alloy nanoparticles with high electrocatalytic performance for methanol oxidation, New J. Chem. 36 (2012) 1774–1780. doi:10.1039/C2NJ40133A.

[59] M. Azarang, A. Shuhaimi, M. Sookhakian, Crystalline quality assessment, photocurrent response and optical properties of reduced graphene oxide uniformly decorated zinc oxide nanoparticles based on the graphene oxide concentration, RSC Adv. 5 (2015) 53117–53128. doi:10.1039/C5RA06123G.

[60] Y. Wei, Y. Zhang, X. Gao, Z. Ma, X. Wang, C. Gao, Multilayered graphene oxide membrane for water treatment: A review, Carbon. 139 (2018) 964–981. doi:10.1016/j.carbon.2018.07.040.

[61] W. Yu, T. (Yet) Yu, N. Graham, Development of a stable cation modified graphene oxide membrane for water treatment, 2D Mater. 4 (2017) 045006. doi:10.1088/2053-1583/aa814c.

[62] J. Ma, D. Ping, X. Dong, Recent Developments of Graphene Oxide-Based Membranes: A Review, Membranes. 7 (2017) 52. doi:10.3390/membranes7030052.

[63]   H. Liu, H. Wang, X. Zhang, Facile Fabrication of Freestanding Ultrathin Reduced Graphene Oxide Membranes for Water Purification, Adv. Mater. 27 (2015) 249–254. doi:10.1002/adma.201404054.

[64]   R.R. Nair, H.A. Wu, P.N. Jayaram, I.V. Grigorieva, A.K. Geim, Unimpeded Permeation of Water Through Helium-Leak–Tight Graphene-Based Membranes, Science. 335 (2012) 442–444. doi:10.1126/science.1211694.

[65]   N. Wei, X. Peng, Z. Xu, Understanding Water Permeation in Graphene Oxide Membranes, ACS Appl. Mater. Interfaces. 6 (2014) 5877–5883. doi:10.1021/am500777b.

[66]   Y. Han, Z. Xu, C. Gao, Ultrathin Graphene Nanofiltration Membrane for Water Purification, Advanced Functional Materials. 23 (2013) 3693–3700. doi:10.1002/adfm.201202601.

[67]   P. Sun, K. Wang, J. Wei, M. Zhong, D. Wu, H. Zhu, Effective recovery of acids from iron-based electrolytes using graphene oxide membrane filters, Journal of Materials Chemistry A. 2 (2014) 7734–7737. doi:10.1039/C4TA00668B.

[68]   L. Wang, N. Wang, J. Li, J. Li, W. Bian, S. Ji, Layer-by-layer self-assembly of polycation/GO nanofiltration membrane with enhanced stability and fouling resistance, Separation and Purification Technology. 160 (2016) 123–131. doi:10.1016/j.seppur.2016.01.024.

[69]   M. Hu, B. Mi, Layer-by-layer assembly of graphene oxide membranes via electrostatic interaction, Journal of Membrane Science. 469 (2014) 80–87. doi:10.1016/j.memsci.2014.06.036.

[70]   N. Rahimi, R.A. Pax, E.M. Gray, Review of functional titanium oxides. I: TiO_2 and its modifications, Progress in Solid State Chemistry. 44 (2016) 86–105. doi:10.1016/j.progsolidstchem.2016.07.002.

[71]   S. Leong, A. Razmjou, K. Wang, K. Hapgood, X. Zhang, H. Wang, TiO2 based photocatalytic membranes: A review, Journal of Membrane Science. 472 (2014) 167–184. doi:10.1016/j.memsci.2014.08.016.

[72]   J.E.S. Haggerty, L.T. Schelhas, D.A. Kitchaev, J.S. Mangum, L.M. Garten, W. Sun, K.H. Stone, J.D. Perkins, M.F. Toney, G. Ceder, D.S. Ginley, B.P. Gorman, J. Tate, High-fraction brookite films from amorphous precursors, Scientific Reports. 7 (2017) 15232. doi:10.1038/s41598-017-15364-y.

[73] D. Reyes-Coronado, G. Rodríguez-Gattorno, M.E. Espinosa-Pesqueira, C. Cab, R. de Coss, G. Oskam, Phase-pure TiO_2 nanoparticles: anatase, brookite and rutile, Nanotechnology. 19 (2008) 145605. doi:10.1088/0957-4484/19/14/145605.

[74] R. Verma, J. Gangwar, A. K. Srivastava, Multiphase TiO 2 nanostructures: a review of efficient synthesis, growth mechanism, probing capabilities, and applications in bio-safety and health, RSC Advances. 7 (2017) 44199–44224. doi:10.1039/C7RA06925A.

[75] B.K. Mutuma, G.N. Shao, W.D. Kim, H.T. Kim, Sol–gel synthesis of mesoporous anatase–brookite and anatase–brookite–rutile TiO_2 nanoparticles and their photocatalytic properties, Journal of Colloid and Interface Science. 442 (2015) 1–7. doi:10.1016/j.jcis.2014.11.060.

[76] N. Venkatachalam, M. Palanichamy, V. Murugesan, Sol–gel preparation and characterization of nanosize TiO_2: Its photocatalytic performance, Materials Chemistry and Physics. 104 (2007) 454–459. doi:10.1016/j.matchemphys.2007.04.003.

[77] S.G. Ullattil, P. Periyat, Sol-Gel Synthesis of Titanium Dioxide, in: Sol-Gel Materials for Energy, Environment and Electronic Applications, Springer, Cham, 2017: pp. 271–283. doi:10.1007/978-3-319-50144-4_9.

[78] S.M. Gupta, M. Tripathi, A review on the synthesis of TiO_2/ nanoparticles by solution route, Cent.Eur.j.Chem. 10 (2012) 279–294. doi:10.2478/s11532-011-0155-y.

[79] D.-S. Lee, T.-K. Liu, Preparation of TiO_2 Sol Using TiCl4 as a Precursor, Journal of Sol-Gel Science and Technology. 25 (2002) 121–136. doi:10.1023/A:1019960211745.

[80] J. Sun, L. Gao, pH Effect on Titania-Phase Transformation of Precipitates from Titanium Tetrachloride Solutions, Journal of the American Ceramic Society. 85 (2002) 2382–2384. doi:10.1111/j.1151-2916.2002.tb00467.x.

[81] Y. Zhu, L. Zhang, C. Gao, L. Cao, The synthesis of nanosized TiO2 powder using a sol-gel method with $TiCl_4$ as a precursor, Journal of Materials Science. 35 (2000) 4049–4054. doi:10.1023/A:1004882120249.

[82] Y. Wang, L. Zhang, K. Deng, X. Chen, Z. Zou, Low Temperature Synthesis and Photocatalytic Activity of Rutile

TiO2 Nanorod Superstructures, J. Phys. Chem. C. 111 (2007) 2709–2714. doi:10.1021/jp066519k.

[83]   W. Zheng, X. Liu, Z. Yan, L. Zhu, Ionic Liquid-Assisted Synthesis of Large-Scale TiO_2 Nanoparticles with Controllable Phase by Hydrolysis of TiCl4, ACS Nano. 3 (2009) 115–122. doi:10.1021/nn800713w.

[84]   H. Zhao, L. Liu, J.M. Andino, Y. Li, Bicrystalline TiO_2 with controllable anatase–brookite phase content for enhanced CO_2 photoreduction to fuels, J. Mater. Chem. A. 1 (2013) 8209–8216. doi:10.1039/C3TA11226H.

[85]   V. Štengl, D. Králová, Photoactivity of brookite–rutile TiO_2 nanocrystalline mixtures obtained by heat treatment of hydrothermally prepared brookite, Materials Chemistry and Physics. 129 (2011) 794–801. doi:10.1016/j.matchemphys.2011.05.006.

[86]   Y. Hu, H.-L. Tsai, C.-L. Huang, Effect of brookite phase on the anatase–rutile transition in titania nanoparticles, Journal of the European Ceramic Society. 23 (2003) 691–696. doi:10.1016/S0955-2219(02)00194-2.

[87]   U.I. Gaya, A.H. Abdullah, Heterogeneous photocatalytic degradation of organic contaminants over titanium dioxide: A review of fundamentals, progress and problems, Journal of Photochemistry and Photobiology C: Photochemistry Reviews. 9 (2008) 1–12. doi:10.1016/j.jphotochemrev.2007.12.003.

[88]   G. Liu, X. Wang, Z. Chen, H.-M. Cheng, G.Q. (Max) Lu, The role of crystal phase in determining photocatalytic activity of nitrogen doped TiO_2, Journal of Colloid and Interface Science. 329 (2009) 331–338. doi:10.1016/j.jcis.2008.09.061.

[89]   D.C. Hurum, A.G. Agrios, S.E. Crist, K.A. Gray, T. Rajh, M.C. Thurnauer, Probing reaction mechanisms in mixed phase TiO_2 by EPR, Journal of Electron Spectroscopy and Related Phenomena. 150 (2006) 155–163. doi:10.1016/j.elspec.2005.01.294.

[90]   Q. Huang, S. Tian, D. Zeng, X. Wang, W. Song, Y. Li, W. Xiao, C. Xie, Enhanced Photocatalytic Activity of Chemically Bonded TiO_2/Graphene Composites Based on the Effective Interfacial Charge Transfer through the C–Ti Bond, ACS Catal. 3 (2013) 1477–1485. doi:10.1021/cs400080w.

[91]   J. Song, Y. Ling, Y. Xie, L. Liu, H. Zhu, One-pot engineering TiO_2 /graphene interface for enhanced adsorption and photocatalytic degradation of multiple organics, Nanotechnology. 29 (2018) 395701. doi:10.1088/1361-6528/aacc56.

[92]   H. Adamu, P. Dubey, J.A. Anderson, Probing the role of thermally reduced graphene oxide in enhancing performance of TiO_2 in photocatalytic phenol removal from aqueous environments, Chemical Engineering Journal. 284 (2016) 380–388. doi:10.1016/j.cej.2015.08.147.

[93]   C. Zhu, G. Liu, K. Han, H. Ye, S. Wei, Y. Zhou, One-step facile synthesis of graphene oxide/TiO_2 composite as efficient photocatalytic membrane for water treatment: Crossflow filtration operation and membrane fouling analysis, Chemical Engineering and Processing: Process Intensification. 120 (2017) 20–26. doi:10.1016/j.cep.2017.06.012.

[94]   C. Xu, A. Cui, Y. Xu, X. Fu, Graphene oxide–TiO_2 composite filtration membranes and their potential application for water purification, Carbon. 62 (2013) 465–471. doi:10.1016/j.carbon.2013.06.035.

[95]   C. Xu, Y. Xu, J. Zhu, Photocatalytic Antifouling Graphene Oxide-Mediated Hierarchical Filtration Membranes with Potential Applications on Water Purification, ACS Appl. Mater. Interfaces. 6 (2014) 16117–16123. doi:10.1021/am5040945.

[96]   J. Wang, Y. Wang, J. Zhu, Y. Zhang, J. Liu, B. Van der Bruggen, Construction of TiO_2@graphene oxide incorporated antifouling nanofiltration membrane with elevated filtration performance, Journal of Membrane Science. 533 (2017) 279–288. doi:10.1016/j.memsci.2017.03.040.

[97]   L.M. Pastrana-Martínez, S. Morales-Torres, J.L. Figueiredo, J.L. Faria, A.M.T. Silva, Graphene oxide based ultrafiltration membranes for photocatalytic degradation of organic pollutants in salty water, Water Research. 77 (2015) 179–190. doi:10.1016/j.watres.2015.03.014.

[98]   X. Yan, Y. Li, F. Du, K. Zhu, Y. Zhang, A. Su, G. Chen, Y. Wei, Synthesis and optimizable electrochemical performance of reduced graphene oxide wrapped mesoporous TiO_2 microspheres, Nanoscale. 6 (2014) 4108–4116. doi:10.1039/C3NR06393C.

[99] H.-H. Huang, K.K.H.D. Silva, G.R.A. Kumara, M. Yoshimura, Structural Evolution of Hydrothermally Derived Reduced Graphene Oxide, Scientific Reports. 8 (2018) 6849. doi:10.1038/s41598-018-25194-1.

[100] L. Zhang, Q. Zhang, H. Xie, J. Guo, H. Lyu, Y. Li, Z. Sun, H. Wang, Z. Guo, Electrospun titania nanofibers segregated by graphene oxide for improved visible light photocatalysis, Applied Catalysis B: Environmental. 201 (2017) 470–478. doi:10.1016/j.apcatb.2016.08.056.

[101] T.-D. Nguyen-Phan, V.H. Pham, E.W. Shin, H.-D. Pham, S. Kim, J.S. Chung, E.J. Kim, S.H. Hur, The role of graphene oxide content on the adsorption-enhanced photocatalysis of titanium dioxide/graphene oxide composites, Chemical Engineering Journal. 170 (2011) 226–232. doi:10.1016/j.cej.2011.03.060.

[102] B. Chen, J. Sha, W. Li, F. He, E. Liu, C. Shi, C. He, J. Li, N. Zhao, Graphene Oxide-Assisted Synthesis of Microsized Ultrathin Single-Crystalline Anatase TiO2 Nanosheets and Their Application in Dye-Sensitized Solar Cells, ACS Appl. Mater. Interfaces. 8 (2016) 2495–2504. doi:10.1021/acsami.5b09058.

[103] W.-S. Wang, D.-H. Wang, W.-G. Qu, L.-Q. Lu, A.-W. Xu, Large Ultrathin Anatase TiO$_2$ Nanosheets with Exposed {001} Facets on Graphene for Enhanced Visible Light Photocatalytic Activity, J. Phys. Chem. C. 116 (2012) 19893–19901. doi:10.1021/jp306498b.

[104] P.J. Huang, H. Chang, C.T. Yeh, C.W. Tsai, Phase transformation of TiO$_2$ monitored by Thermo-Raman spectroscopy with TGA/DTA, Thermochimica Acta. 297 (1997) 85–92. doi:10.1016/S0040-6031(97)00168-8.

[105] G. Jiang, Z. Lin, C. Chen, L. Zhu, Q. Chang, N. Wang, W. Wei, H. Tang, TiO$_2$ nanoparticles assembled on graphene oxide nanosheets with high photocatalytic activity for removal of pollutants, Carbon. 49 (2011) 2693–2701. doi:10.1016/j.carbon.2011.02.059.

[106] E. Cruz-Silva, X. Jia, H. Terrones, B.G. Sumpter, M. Terrones, M.S. Dresselhaus, V. Meunier, Edge–Edge Interactions in Stacked Graphene Nanoplatelets, (2013). doi:10.1021/nn4004204.

[107] M. Zeiger, N. Jäckel, V. N. Mochalin, V. Presser, Review: carbon onions for electrochemical energy storage, Journal of Materials Chemistry A. 4 (2016) 3172–3196. doi:10.1039/C5TA08295A.

[108] S. Zhang, J. Niu, H. Song, L. Zhu, J. Zhou, X. Chen, J. Liu, S. Hong, R. Song, Can closed shell graphitic materials be exfoliated? Defect induced porphyra-like graphene from the cooperation of activation and oxidation, J. Mater. Chem. A. 1 (2013) 14103–14107. doi:10.1039/C3TA13383D.

[109] J. Zhang, Z. Xiong, X.S. Zhao, Graphene–metal–oxide composites for the degradation of dyes under visible light irradiation, J. Mater. Chem. 21 (2011) 3634–3640. doi:10.1039/C0JM03827J.

[110] D. Peng, W. Qin, X. Wu, J. Wu, Y. Pan, Improvement of the resistance performance of carbon/cyanate ester composites during vacuum electron radiation by reduced graphene oxide modified TiO2, RSC Adv. 5 (2015) 77138–77146. doi:10.1039/C5RA11113G.

[111] G. Rajender, J. Kumar, P.K. Giri, Interfacial charge transfer in oxygen deficient TiO_2-graphene quantum dot hybrid and its influence on the enhanced visible light photocatalysis, Applied Catalysis B: Environmental. 224 (2018) 960–972. doi:10.1016/j.apcatb.2017.11.042.

[112] P. Chen, L. Wang, P. Wang, A. Kostka, M. Wark, M. Muhler, R. Beranek, $CNT-TiO_2-\delta$ Composites for Improved Co-Catalyst Dispersion and Stabilized Photocatalytic Hydrogen Production, Catalysts. 5 (2015) 270–285. doi:10.3390/catal5010270.

[113] O. Akhavan, E. Ghaderi, Photocatalytic Reduction of Graphene Oxide Nanosheets on TiO_2 Thin Film for Photoinactivation of Bacteria in Solar Light Irradiation, J. Phys. Chem. C. 113 (2009) 20214–20220. doi:10.1021/jp906325q.

[114] F. Sordello, G. Zeb, K. Hu, P. Calza, C. Minero, T. Szkopek, M. Cerruti, Tuning TiO_2 nanoparticle morphology in graphene–TiO 2 hybrids by graphene surface modification, Nanoscale. 6 (2014) 6710–6719. doi:10.1039/C4NR01322K.

[115] Y. Chen, H. Gao, J. Xiang, X. Dong, Y. Cao, Enhanced photocatalytic activities of TiO_2-reduced graphene oxide nanocomposites controlled by TiOC interfacial chemical bond,

Materials Research Bulletin. 99 (2018) 29–36. doi:10.1016/j.materresbull.2017.08.054.

[116] L. Li, L. Yu, Z. Lin, G. Yang, Reduced TiO_2-Graphene Oxide Heterostructure As Broad Spectrum-Driven Efficient Water-Splitting Photocatalysts, ACS Appl. Mater. Interfaces. 8 (2016) 8536–8545. doi:10.1021/acsami.6b00966.

[117] R. López, R. Gómez, Band-gap energy estimation from diffuse reflectance measurements on sol–gel and commercial TiO2: a comparative study, J Sol-Gel Sci Technol. 61 (2012) 1–7. doi:10.1007/s10971-011-2582-9.

[118] M. Khannam, S. Sharma, S. Dolui, S.K. Dolui, A graphene oxide incorporated TiO_2 photoanode for high efficiency quasi solid state dye sensitized solar cells based on a poly-vinyl alcohol gel electrolyte, RSC Adv. 6 (2016) 55406–55414. doi:10.1039/C6RA07577K.

[119] V. Štengl, S. Bakardjieva, T.M. Grygar, J. Bludská, M. Kormunda, TiO_2-graphene oxide nanocomposite as advanced photocatalytic materials, Chemistry Central Journal. 7 (2013) 41. doi:10.1186/1752-153X-7-41.

[120] M. Minella, F. Sordello, C. Minero, Photocatalytic process in TiO2/graphene hybrid materials. Evidence of charge separation by electron transfer from reduced graphene oxide to TiO_2, Catalysis Today. 281 (2017) 29–37. doi:10.1016/j.cattod.2016.03.040.

[121] G. Malekshoar, K. Pal, Q. He, A. Yu, A.K. Ray, Enhanced Solar Photocatalytic Degradation of Phenol with Coupled Graphene-Based Titanium Dioxide and Zinc Oxide, Ind. Eng. Chem. Res. 53 (2014) 18824–18832. doi:10.1021/ie501673v.

[122] M. Aleksandrzak, P. Adamski, W. Kukułka, B. Zielinska, E. Mijowska, Effect of graphene thickness on photocatalytic activity of TiO_2-graphene nanocomposites, Applied Surface Science. 331 (2015) 193–199. doi:10.1016/j.apsusc.2015.01.070.

[123] W.-S. Hung, C.-H. Tsou, M. De Guzman, Q.-F. An, Y.-L. Liu, Y.-M. Zhang, C.-C. Hu, K.-R. Lee, J.-Y. Lai, Cross-Linking with Diamine Monomers To Prepare Composite Graphene Oxide-Framework Membranes with Varying d-Spacing, Chem. Mater. 26 (2014) 2983–2990. doi:10.1021/cm5007873.

[124] K.H. Chu, Y. Huang, M. Yu, J. Heo, J.R.V. Flora, A. Jang, M. Jang, C. Jung, C.M. Park, D.-H. Kim, Y. Yoon, Evaluation of graphene oxide-coated ultrafiltration membranes for humic acid removal at different pH and conductivity conditions, Separation and Purification Technology. 181 (2017) 139–147. doi:10.1016/j.seppur.2017.03.026.

[125] M.F. Craciun, S. Russo, M. Yamamoto, J.B. Oostinga, A.F. Morpurgo, S. Tarucha, Trilayer graphene is a semimetal with a gate-tunable band overlap, Nature Nanotechnology. 4 (2009) 383–388. doi:10.1038/nnano.2009.89.
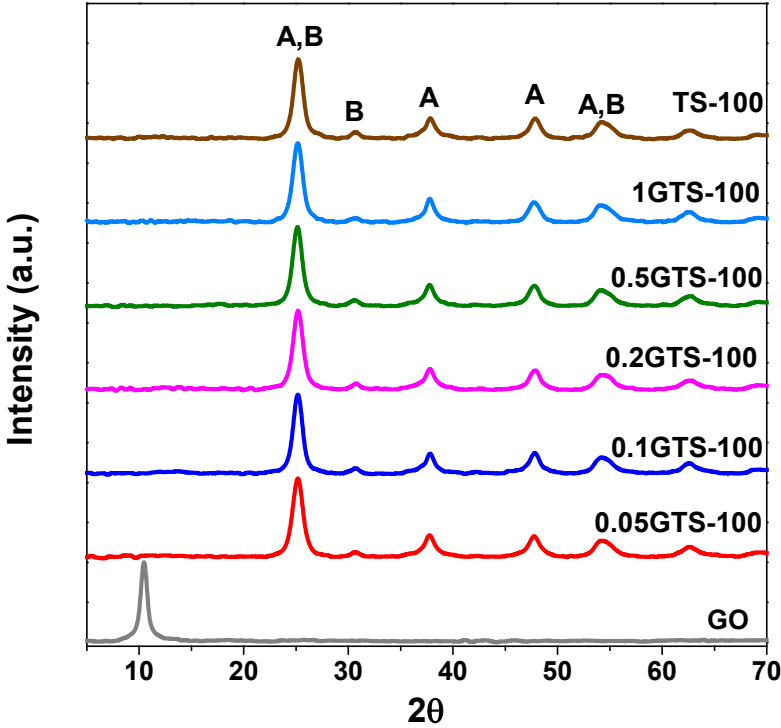
LIST OF PUBLICATION

PUBLICATIONS IN PEER-REVIEW JOURNALS

1) **U. Naknikham**, V. Boffa, G. Magnacca, A. Qiao, L. R. Jensen, Y. Yue, 2017, "Mutual-stabilization in chemically bonded graphene oxide–TiO_2 heterostructures synthesized by a sol–gel approach", *RSC Advances*, 7, 41217-41227 (2016).
2) **U. Naknikham**, G. Magnacca, A. Qiao, P.K. Kristensen, V. Boffa, Y. Yue, "Phenol abatement by titanium dioxide photocatalysts: effect of the graphene oxide loading" (to be submitted).
3) **U. Naknikham**, G. Magnacca, A. Qiao, P.K. Kristensen, V. Boffa, Y. Yue, "Phenol Abatement by $GO-TiO_2$ and $rGO-TiO_2$ Photocatalsts" (under reparation).

CONFERENCE CONTRIBUTIONS

1) U. Naknikham, V. Boffa, Y. Yue. 2017, In-situ sol-gel synthesis of titanium dioxide-graphene oxide heterostructures for water purification technologies. Poster presentation: *12th Pacific Rim Conference on Ceramic and Glass Technology including Glass & Optical Materials Division Meeting,*Hawaii, USA (2017).
2) U. Naknikham, V. Boffa, Y. Yue. 2017. Enhanced bonding between TiO2-Graphene oxide. Poster presentation: *Graphene Week 2017,* Athens, Greece (2017).
3) U. Naknikham, E. Marino, V. Boffa, Y. Yue. 2017. Graphene-based materials for photocatalysis and membrane filtration. Poster presentation: *17TH Nordic Filtration Symposium,* Aalborg, Denmark (2018).

Appendix A. XRD driffractogram of GO, TS, and GTS-100 composites with different GO loading